

This manuscript is a preprint.

Title: Relative contributions of water level components to extreme water levels along the United States
5 Southeast Atlantic Coast from a regional-scale water level hindcast

Authors:

- Kai Parker (USGS. kaparker@usgs.gov)
- Li Erikson (USGS. lerikson@usgs.gov)
- 10 • Jenny Thomas (USGS. jathomas@usgs.gov)
- Kees Nederhoff (Deltares USA. kees.nederhoff@deltares-usa.us)
- Patrick Barnard (USGS. pbarnard@usgs.gov)
- Sanne Muis (Institute for Environmental Studies (IVM). sanne.muis@vu.nl)

15

Statement:

This manuscript is a non-peer reviewed preprint submitted to EarthArXiv.

This manuscript has been submitted to Natural Hazards for review.

20 Subsequent versions of this manuscript may have different content. If accepted, the final version of
this manuscript will be available via the 'Peer-reviewed Publication DOI' link via this webpage.

Relative contributions of water level components to extreme water levels along the United States Southeast Atlantic Coast from a regional-scale water level hindcast

Kai Parker ¹, Li Erikson ², Jenny Thomas³, Kees Nederhoff⁴, Patrick Barnard⁵, Sanne Muis^{6,7}

¹ USGS, Pacific Coastal and Marine Science Center, Santa Cruz, USA. (kaparker@usgs.gov) ORCID-ID: 0000-0002-0268-3891

² USGS, Pacific Coastal and Marine Science Center, Santa Cruz, USA. (lerikson@usgs.gov) ORCID-ID: 0000-0002-8607-7695

³ USGS, Pacific Coastal and Marine Science Center, Santa Cruz, USA. (jathomas@usgs.gov) ORCID-ID: 0000-0002-8338-0146

⁴ Deltares USA, 8601 Georgia Ave., Silver Spring, MD 20910, USA, (kees.nederhoff@deltares-usa.us) ORCID-ID: 0000-0003-0552-3428

⁵ USGS, Pacific Coastal and Marine Science Center, Santa Cruz, USA. (pbarnard@usgs.gov) ORCID-ID: 0000-0003-1414-6476

⁶ Deltares, Delft, Netherlands

⁷ Institute for Environmental Studies (IVM), Vrije Universiteit Amsterdam, Amsterdam, Netherlands (sanne.muis@vu.nl) ORCID-ID: 0000-0002-8145-0171

Corresponding Author: Kai Parker (kaparker@usgs.gov)

Abstract:

A 38-year hindcast water level product is developed for the United States Southeast Atlantic coastline from the entrance of Chesapeake Bay to the southeast tip of Florida. The water level modelling framework utilized in this study combines a global-scale hydrodynamic model (Global Tide and Surge Model, GTSM-ERA5), a novel ensemble-based tide model, a parameterized wave setup model, and statistical corrections applied to improve modelled water level components. Corrected water level data are found to be skillful, with an RMSE of 13 cm, when compared to observed water level measurement at tide gauge locations. The largest errors in the hindcast are location-based and typically found in the tidal component of the model. Extreme water levels across the region are driven by compound events, in this case referring to combined surge, tide, and wave forcing. However, the relative importance of water level components varies spatially, such that tides are found to be more important in the center of the study region, non-tidal residual water levels to the north, and wave setup in the north and south. Hurricanes drive the most extreme water level events within the study area, but non-hurricane events define the low to mid-level recurrence interval water level events. This study presents a robust analysis of the complex oceanographic factors that drive coastal flood events. This dataset will support a variety of critical coastal research goals including research related to coastal hazards, landscape change, and community risk assessments.

60 Keywords: Extreme Sea levels, Coastal Flooding, Regional Hindcast, Wave Setup, Water Levels, Extreme Events, Compound
Events

1. Introduction

An ongoing challenge in water level modelling is the trade-off between scale and skill. Generally, larger scale products (regional to global) are forced to trade accuracy for increased spatial and temporal coverage (Vousdoukas et al.,
65 2016). Skill is often lost for larger scale products because of coarser resolution, parameterization of local scale processes, computational costs, and reduced physics (Fewtrell et al., 2008; Maraun et al., 2010). This trade-off is problematic because, especially in the field of coastal hazards, there remains a strong need for large scale data that are relevant at local scale (Ward et al., 2015). In terms of spatial coverage, a complete understanding of risk and how to allocate resources at governmental levels requires a regional understanding of hazards that extends beyond isolated local study sites. Furthermore, most
70 communities outside of large urban centers lack the resources and/or technical expertise to develop local hazard assessments. Therefore, products that cover large geographic regions with planning-level granularity provide both a more unified and equitable resource for understanding coastal hazards by making data available for every coastal community. Beyond large spatial scales, long temporal records are required for constraining extremes (Wahl et al., 2017), understanding changes to hazards over time, and for characterizing decadal to interannual scale variability (Weisse et al. 2014). Overall, there remains
75 a strong motivation for developing and improving large scale models that are both efficient and accurate for coastal hazards research.

This study explores the recently developed Global Tide and Surge Model ERA5 dataset (GTSM-ERA5, Muis et al., 2016, 2020) for predicting coastal water levels along the Southeast Atlantic coastline of the United States. Previous water level hindcast analyses in the region have been limited spatially to tide gauge locations (Ezer and Atkinson, 2014; Davis and
80 Vinogradova, 2017), specific study sites (e.g., New York, Georgas et al., 2016), or focused only on specific types of events such as Hurricanes (Marsooli et al., 2018) or extratropical events such as Nor'easters (Lin et al., 2019). This data gap is primarily due to computational constraints and the scale/skill trade-off discussed above. GTSM, created using Delft3D Flexible Mesh (Kernkamp et al. 2011) by Deltares, narrows this tradeoff for nearshore water level modelling by leveraging a variety of recent modelling developments. These include unstructured meshes and parallel processing, in combination with increased
85 computational processing power. This study builds on recent work by Muis et al. (2016), who found that GTSM successfully reproduced observed daily water level maxima across a global sample of tide gauges as well as in the U.S. Atlantic region (Muis et al., 2019). In addition, Dullaart et al. (2020) and Bloemendaal et al. (2019) showed acceptable skill of GTSM, forced with ERA5 resolution winds (31 km), in simulating surge levels produced by tropical cyclones. Combined, these recent works suggest that GTSM-ERA5 is a viable source for developing a detailed water level hindcast in the study region.

90 In this study, GTSM-ERA5 data were combined with estimates of wave setup to produce a hindcast scale (~38 years)
dataset of water levels with a regional coverage area (1000+ kilometers) along the U.S. Southeast Atlantic Coast. A water level
hindcast of this sort does not exist in the region and is expected to facilitate a variety of coastal research goals, such as coastal
hazard assessments. A series of statistical corrections were developed to improve model skill for individual signals (astronomic
tides, monthly mean sea levels, non-tidal residual, seasonality, and wave setup; all signals defined below in section 3) that
95 contribute to the GTSM-ERA5 derived water levels in the study region. Following application of these corrections, the spatial
variability of individual component contributions to the total water level, including wave setup, were quantified, and compared
to gain further insight into processes contributing to flooding across the region. Results focus on extremes, as a primary interest
for coastal hazard assessments, and their contributing signals. Overall, this modelling framework both accurately and
efficiently reproduces coastal water levels in a complex setting influenced by both tropical and extratropical storm systems,
100 and thus is a viable approach for examining water levels at both large spatial and temporal scales.

This paper is organized with the initial section (section 2) describing the regional scope of the produced dataset and
the utilized observational and reanalysis data. Section 3 presents methods used to bias correct and decompose the time-series
into astronomic tides, seasonality, monthly mean sea levels (MMSL), and non-tidal residuals (NTR). Section 3 also details the
method for calculating wave setup, an additional critical component for experienced total water levels along the coast. The
105 next section (section 4) discusses model-observation comparisons using regional tide gauges, with model performance
evaluated both for signals contributing to water levels and for combined water levels. Finally, the paper moves into results
(section 5) and discussion (section 6).

2. Study Sites and Observations

2.1 Study Region

110 This study focuses on the Southeast United States Atlantic coastline, extending 1,500 km from the southeastern tip
of Florida north to the entrance to Chesapeake Bay (Figure 1). This region covers a diverse range of coastal systems including
sandy beaches, bays, marshes, and barrier islands. This range of coastal morphologies is closely coupled with the variable
ocean climate along the coast, as explored by this study. For example, barrier island characteristics are at the most basic level
controlled by tidal range and wave climate (Hayes, M.O., 1979). The coastal zone in the southern portion of this region
115 (Florida) is highly developed whereas the north section represents a more mixed land usage (Titus et al., 2009). Low lying
vulnerable infrastructure is ubiquitous along the coast (e.g., Armstrong and Lazarus, 2019; Bin et al., 2011; Wdowinski et al.,
2018; Ezer and Atkinson, 2014), and approximately 14 million residents live in the coastal counties spanning the study region
(US Census, 2021).

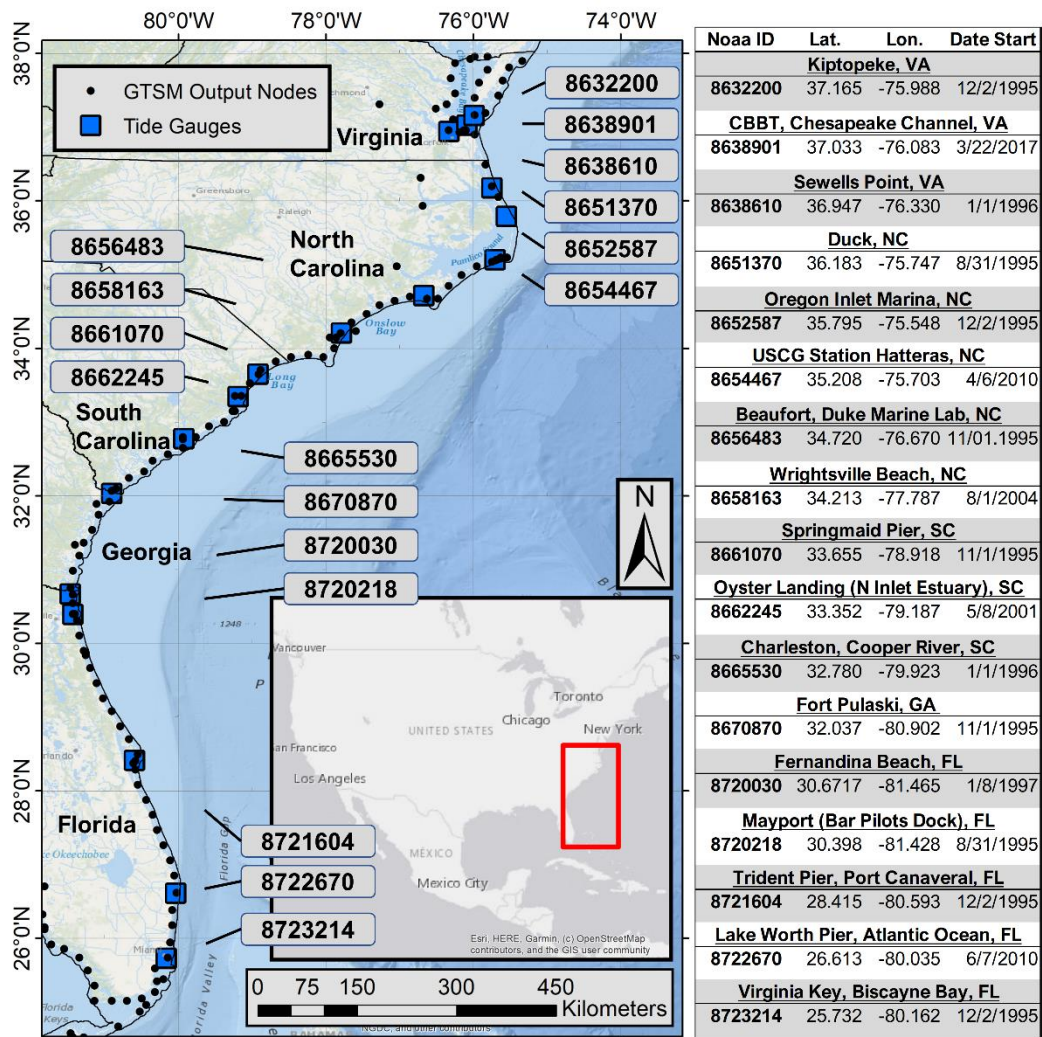


Figure 1: Study region with GTSM-ERA5 output locations marked as black circles and tide gauge locations marked as blue squares. Grey labels denote NOAA designated tide gauge station IDs. Information on tide gauges, including ID number, latitude, longitude, and the date when observations start, are listed in the table to the right of the map.

120

125 2.2 Observational/Reanalysis Data

2.2.1 ERA5

ERA5 (Hersbach et al., 2018; Hersbach et al., 2020) atmospheric and ocean wave fields were used as forcing for the GTSM-ERA5 dataset (Muis et al., 2020) and wave setup parameterization, respectively. ERA5 represents a significant improvement over previous global reanalysis products through increased temporal (hourly) and spatial (31-km grid) resolution, improvements to model physics, and a drastic increase in assimilated data. Validations of ERA5 meteorological products have

130

shown significant improvements in model predictive skill over the previous ERA-Interim product (Rivas and Stoffelen, 2019; Haiden et al., 2019).

135 A variety of wave hindcast and reanalysis products are available with data within the study region. The ERA5 wave product (Hersbach et al., 2018; Hersbach et al., 2020) was selected primarily for consistency with the hydrodynamics, which were forced with ERA5 atmospheric fields. Additionally, ERA5 improves upon other available wave hindcasts by including hourly assimilation of altimeter derived significant wave height data. Several studies have shown as good or better skill by ERA5 compared to other wave products (Erikson, et al. In Review; Timmermans et al., 2020).

2.2.2 Tide Gauges

140 NOAA's tide gauge database (<https://tidesandcurrents.noaa.gov/>) was used to validate the GTSM-ERA5 water levels. This study benefits from the region's relatively high density (seventeen) of long-term tide gauge records. The full available 6-minute observed water level intervals were used (Figure 1).

3. Methods

145 This study features a significantly simplified modelling framework than previous studies of this scale. Specifically, the unstructured nature of Delft3D Flexible Mesh (utilized in GTSM-ERA5) eliminates the need for various levels of model nesting to downscale global level oceanographic data to the local scale. Furthermore, the increased resolution and quality of the ERA5 reanalysis product reduces the need for dynamic downscaling of atmospheric data. Therefore, the full methods of this study reduce to a series of statistical corrections to the GTSM data and a wave setup model. These components are detailed in the following sections.

3.1 Hydrodynamics

150 Modelling of nearshore water levels is performed using the Global Tide and Surge Model version 3.0 (GTSMv3.0) (Muis et al., 2020; Muis et al., 2022). GTSMv3.0 is a global scale implementation of Delft3D Flexible Mesh (Kernkamp et al., 2011) developed by Deltares. The unstructured nature of the GTSM grid allows for variable mesh resolution ranging from approximately 2.5 km along the U.S. coastlines to 25 km in the deep ocean. While resolution is improved from previous global models, nearshore resolution is still often insufficient to resolve small-scale coastal features. The overall mesh is over 5 million grid cells with bathymetry set using the General Bathymetric Chart of the Ocean (GEBCO, 2014) bathymetry dataset, which provides global 30 arc-second bathymetry. GTSM is a global model so has no open ocean boundaries, only atmospheric. Therefore, tides are generated internally through tidal generating forces for over 60 harmonics (Apecechea et al., 2017). Atmospheric forcing is provided through wind and sea level pressure fields using the ERA5 climate reanalysis (Hersbach et al., 2018; Hersbach et al., 2020). The 38-year hindcast dataset (1979-2017) produced using GTSM forced with ERA5 is called
160 GTSM-ERA5 (which is used for the rest of this paper). GTSM-ERA5 was configured with output stations at approximately

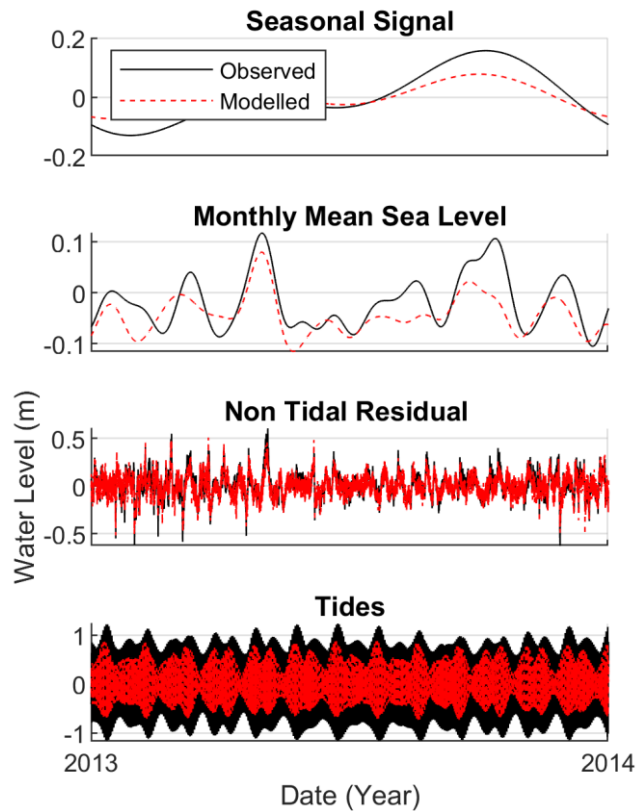
20 km resolution along the coastline (see Figure 1). These stations were supplemented with outputs co-located at tide gauge locations as well as increased station resolution in bathymetrically complex regions. Co-located output/tide gauge locations allow for multi-decadal scale model-observation comparisons at various locations within the study region.

165 GTSM-ERA5 and NOAA tide gauge water levels were decomposed into a subset of contributing signals: tides, seasonality, non-tidal residual (NTR), and monthly mean sea level (MMSL). Water levels were separated into 4 components to gain insight into processes contributing to high water levels, as well as to better develop methods for process specific corrections to each signal. The decomposition of water levels was accomplished by first separating water levels into tides* and NTRs*, labeled here with a star as these signals are intermediate and further separated. For GTSM-ERA5, two different model runs were performed, one with full forcing and one with tidal only forcing. Modelled NTRs* were calculated by subtracting modelled tides from simulations with full forcing. For tide gauge stations, observed NTRs* were calculated by subtracting NOAA-predicted tide signals from observed water levels. After separating tidal* and NTR* water levels, each of these signals were split into two additional signals. NTR* was separated into a MMSL component and a NTR component (as defined as NTR* with MMSL removed). Tidal* water levels were separated into a seasonal signal and a tidal signal (as defined as tidal* with seasonality removed). The definition and calculation of the MMSL and seasonal signal is described below in section 3.1.3 and 3.1.4.

175 Here we define the still water level (SWL) as the linear superposition of four components (eqn. 1a): astronomic tides, astronomic seasonal cycles, non-tidal residuals, and monthly mean sea levels. Note that the SWL varies in time but includes the term ‘still’ to distinguish the elevations from the addition of wave setup or runup. The separation of SWL signals can be visually seen for both the observed and raw GTSM-ERA5 data in Figure 2. The addition of wave setup (see section 3.2) to the SWL is termed “mean water levels” or MWLs (eqn. 1b) (FEMA, 2015).

$$\mathbf{Still\ Water\ Level\ (SWL) = Tides + Seasonality + NTR + MMSL} \quad \mathbf{(Eqn.\ 1a)}$$

$$\mathbf{Mean\ Water\ Level\ (MWL) = SWL + wave\ setup} \quad \mathbf{(Eqn.\ 2b)}$$



185

Figure 2: Example comparison of observed and modelled SWL signals at tide gauge 8665530 (Charleston, SC). Displayed timeseries are before statistical correction (raw GTSM-ERA5 data). Note that signals are decomposed as per eqn. 1a, so tides have seasonality removed and NTR has MMSL removed.

190 3.1.1 SLR

Observed SWLs across the study region were found to have a statistically significant trend (ranging from 2-4 mm/year). At the scale of the considered 38-year period, this trend was considered contributable to sea level rise (SLR) rather than short term variability. Global SLR was included in GTSM-ERA5 (both in the full forcing and tide-only runs) to capture non-linear effects of SLR on hydrodynamics (Idier et al., 2019; Wahl, 2017). Modelled local trends in water levels were found to be consistent with observed trends at the tide gauges and satellite altimetry (Sweet et al., 2022). This study takes the approach of removing the trend in SWL, both from the modelled and observed timeseries. A linear regression was fit to the entire modelled and observed timeseries at each output location and then removed from the water level timeseries. SLR was removed for a variety of reasons, the first being that it allows for a stationary analysis where extremes (as well as other SWL statistics) are not a function of time. Secondly, the approach allows for validating the effectiveness of the modelling framework separate

200 from SLR. In the future SLR becomes a source of significant uncertainty (Sweet et al., 2022), so it is valuable to assess the skill of the modelling framework separate from the SLR component.

3.1.2 Tides

205 The tidal component of SWL is the largest error fraction, with respect to Root-Mean-Square-Error (RMSE), in GTSM-ERA5 data at most tide gauge comparison points. Therefore, an alternative tidal correction model was developed. The periodic nature of tides represents a unique problem in that corrections in the time domain are unlikely to be effective. As an example, a small error in tidal harmonic phase (shifting the tidal timeseries) will create a cyclic over and under bias that is difficult to correct with time domain methods targeted at systematic bias. Corrections to tidal harmonics in the frequency domain are therefore more effective. This has the additional benefit of reducing the complexity of the correction since a tidal harmonic can be fully represented by only two parameters (phase and amplitude).

210 A variety of openly available and well validated global tide models were selected to improve modelled tidal water levels. A subset of best performing global tide models (Stammer et al., 2104; Seifi et al., 2019) were downloaded and compared to NOAA predicted tides at all tide gauges within the study region (see Table 1). Older versions of both the TPXO and FES model series were included as some studies have found that these older versions may perform better than the newest version in certain regions (Lyard et al., 2021). For our study site, the FES2014 (Lyard et al., 2006) and TPXO v9.2 (Egbert et al., 2010) 215 were found to be the best performing models, with approximately equal skill on average across the region. This said, model performance was found to depend on location.

220 **Table 1: Comparison of model RMSE (in centimeters) for all tide gauges (rows) and all tidal model products (columns) tested as part of this study. The final column is the model performance of the Ensemble method. Bold values represent the best performing model at a specific tide gauge station.**

Station ID	<u>Tidal Model Performance vs. Tide Gauges (RMSE, cm)</u>					
	GTSM	TPXO8	TPXO9.2	FES2012	FES2014	Ensemble
8632200	10.8	20.2	3.3	11.9	9.2	4
8638901	11.3	20.4	4.8	5.8	3	2.9
8638610	10.4	12.3	14	11.1	5	2.9
8651370	17	33	24.6	29.8	9.1	17.4
8652587	14	4.5	6.7	14.4	26.7	10.5
8654467	20.2	4.7	10.7	21.5	18.4	15.9
8656483	14.3	31.4	11.6	10	12.1	6.7
8658163	20.8	32	3.9	4.5	3.7	5.2
8661070	26.8	50.4	6	5.2	4.6	8.2
8662245	27.3	46.2	22.4	30.3	27	23.6
8665530	29.6	42	7.5	16	12	8.5

8670870	37	52.8	12.1	23.5	12.4	14.4
8720030	35.5	33.9	17.8	29.5	21.2	17.7
8720218	20.4	29.7	14.4	16.3	14.3	9.9
8721604	19	34.4	2.6	5.8	3.1	5.7
8722670	14.4	23.9	2.1	5.8	2.2	4.2
8722956	12.3	19.1	2.1	7.4	2.3	3.6
8723214	7.1	8.5	17.4	4.7	7.8	2.6
Average	19.3	27.7	10.2	14.1	10.8	9.1

225 A blended product was created to take advantage of the best parts of each model in the ensemble. Conceptually this is like Global Climate Model ensembles where the mean of multiple models can be considered more robust than any individual model. The developed strategy predicts tides using a weighted mean of all tidal harmonics (both phase and amplitude). The weight for each model was determined by the average performance of that model across all tide gauges. More specifically, each tidal constituent amplitude / phase was assigned its own weighting of the contributing models as determined by the performance of that model. Eqn. 2 details the utilized weighting scheme:

230

$$W_{i,j} = \left(\frac{1}{MAE_{i,j}} \right) / \sum_{j=1}^n MAE_{i,j} \quad (\text{Eqn. 3})$$

where:

W: Individual model weighting for the specific harmonic phase or amplitude

MAE: Mean Absolute Error across all tide gauges for the specific harmonic phase/amplitude

235 **i**: index for each amplitude and phase of tidal harmonics

j: index for models contributing to the tidal ensemble

n: number of models available for the specific amplitude/phase of the tidal harmonic

The numerator of eqn. 2 penalizes the model's weight in the weighted average for a larger MAE. The denominator normalizes the weighting so that the sum of weights is 1.

240

Tides were computed by extracting each tide model's phase and amplitude for all available tidal harmonics at each GTSM-ERA5 output location. As GTSM-ERA5 data are only available as timeseries, the phase and amplitudes were determined by performing a harmonic analysis using Utide software (Codiga, 2011,2021) at each output location. While generally found to perform less well than using results from the FES and TPX models, GTSM-ERA5 was included within the ensemble to integrate nonlinear interactions between tide and surge. A new set of phase and amplitudes were generated by

245

combining the ensemble phase and amplitudes through the weighting scheme detailed above. Tides were then recomputed using this new set of phase and amplitudes using the t_tide software package (Pawlowicz et al., 2002).

3.1.3 Astronomic Seasonality

Seasonality was defined for this project as the astronomically derived SA (Solar Annual; period of 365 days) and SSA (Solar Semi-Annual; period of 183 days) harmonics within the tidal component. This differs from other study definitions of seasonality, for example by NOAA (NOAA, 2009), who analyses the yearly average of MMSL. NOAA's definition would therefore include seasonal variations in NTR in addition to tides. Seasonality was included as an individual component in the modelling framework for a variety of reasons. The first was that seasonality was determined to be a major source of error in GTSM-ERA5 data. Secondly, seasonality was found to be insufficiently reproduced using the tidal model ensemble method (see section 3.1.2). This was primarily because most of the selected tidal models do not include seasonal harmonics. Only FES2014 and GTSM-ERA5 contained seasonality as a tidal component, and both were found to greatly underpredict variability in the study region, necessitating the need for corrections to this parameter.

A simple linear regression-based shift of the seasonal harmonic phase and amplitude was selected as the statistical correction methodology. The regression was developed using a single explanatory variable, station latitude, which was implemented to account for along coast variations in the seasonal error (see eqn. 3).

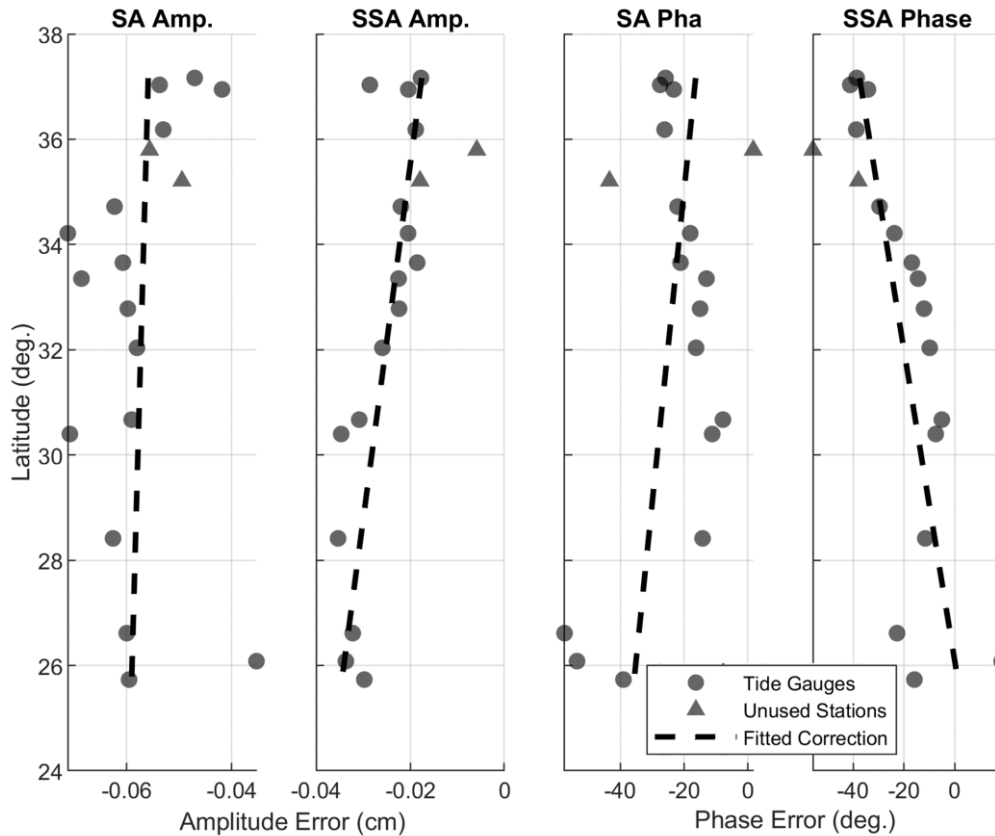
$$Corr = B_1 Lat + B_2 \quad (Eqn. 4)$$

where: **Lat**: latitude in degrees of the tide gauge location.

B: least squares fitted regression coefficients.

Corr: Correction applied to the phase/amplitude of the Seasonal Harmonic.

Each harmonic amplitude and phase error (the response variable in the regression) was fitted with an individual linear regression based on the error at tide gauges within the region. This can be seen visually in Figure 3. Notably, two gauges were omitted from the linear regression fitting (station 8652587 and 8654467; Oregon Inlet, NC, and Hatteras, NC) due to poor comparison between GTSM-ERA5 data and observations. A sensitivity analysis showed that inclusion of these stations did not significantly affect regression coefficient estimates. Rather, these stations were omitted more for consistency with the handling of these outlier stations in other parts of the modelling framework.



275 **Figure 3: Visual representation of linear corrections to the SA (Solar Annual; period of 365 days) and SSA (Solar Semi-Annual; period of 183 days) harmonics amplitude (subpanel 1 & 2) and phase (subpanel 3 & 4) as a function of latitude. Dashed lines are the linear relationship fitted to the circles which plot the error at individual tide gauge stations. Triangles are stations that were not used for fitting the correction.**

3.1.4 Monthly Mean Sea Level

280 Monthly Mean Sea Level (MMSL) was derived in this study using a low-pass filter on SWLs after the removal of tides and seasonality. A filtering approach was chosen instead of the more conventional “monthly means” method as a more complete method of removing low frequency energy from the signal. The monthly means definition is somewhat complicated when removed from the overall signal, requiring interpolation between months to a finer temporal resolution to remove offsets. Furthermore, the resulting effects in the frequency domain are complicated with removal and retention of periodic signals
 285 being based on the relationship of the mean and signal’s periods (Wang et al., 2009). This study instead uses a 4th order butterworth filter with cut-off frequency of 0.3858 μ Hz (1/30 days) applied using a backward forward methodology to remove phase shift. The resulting MMSL timeseries was found to be a cleaner representation of low frequency energy than the classic monthly means definition.

It was decided to separate MMSL from the NTR signal for additional insight into GTSM-ERA5's performance. MMSL is often controlled by different processes than local NTR. The U.S. East Atlantic has seen a recent surge of research on MMSL after it was noticed that tide gauge records in the region showed a significant acceleration of SLR, approximately 3-4 times greater than the global average (Sallenger et al., 2012). The exact cause of this increase in MMSL remains debated but has been tied to a variety of processes, including regional atmospheric patterns (Andres et al., 2013; Domingues et al., 2018; Zhao and Johns, 2014), Gulf Stream dynamics (Andres et al., 2013; Domingues et al., 2018; Ezer et al., 2013; Kopp, 2013; Yin and Goddard, 2013), ice sheet decline (Davis and Vinogradova, 2017), and climate patterns such as the North Atlantic Oscillation (NAO) (Ezer and Atkinson, 2014; Kenigson et al., 2018; Kopp, 2013). GTSM-ERA5 is not capable of capturing all of these potential contributors to MMSL, so the signal was separated from higher frequency NTR for further investigation and potentially for correction.

Despite limits to the physics included in GTSM-ERA5, further investigation found that MMSL variability was reasonably well represented by GTSM-ERA5. GTSM-ERA5's MMSL signal was found to have a small bias (~ 3 cm) in the mean MMSL value in comparison to observations. Therefore, MMSL was post-processed by adding 3 cm. With GTSM-ERA5 skill found to be sufficient, no additional statistical corrections were applied to the MMSL component.

3.1.5 Non-Tidal Residual

Non-tidal residual (NTR) in this study was defined as conventional NTR* (SWL minus tides), but additionally with MMSL removed (see section 3.1.4). Therefore, NTR is herein defined as all NTR energy with a frequency higher than 0.3858 μ Hz. GTSM-ERA5 was found to have significant skill at resolving NTR across the study region with only a few problematic tide gauges. Tide gauges 8652587 (Oregon Inlet, NC) and 8654467 (Hatteras, NC) were flagged as outliers in comparisons to GTSM-ERA5. Further investigation showed that these gauges are located behind thin barrier islands with small inlet channels. While GTSM-ERA5 leverages unstructured meshing to have very high coastal resolution for a global model, the resolution is still on the order of 2.5 km. This resolution remains insufficient to resolve small scale coastal features (such as thin barrier islands or small channels). While sub-resolution features make model-observation comparisons at the flagged tide gauges problematic, it is less of a problem for the overall study and produced hindcast dataset. In the resulting analysis, GTSM-ERA5 data are only examined in the nearshore open-coast region. The use of only open-coast GTSM-ERA5 data restricts the study's conclusions to the open coast region and means that GTSM-ERA5 does not need to be, nor is expected to be, skillful within back bays.

Overall, GTSM-ERA5 NTR data were found to be reasonably skillful in comparison to tide gauges (average RMSE of 6 cm). A statistical correction was performed due to the importance of NTR during flooding events. Additionally, extreme SWLs were found to be significantly underpredicted, a result in agreement with results by Muis et al. (2017). Underprediction of extremes is particularly undesirable due to the importance of these events from a coastal hazard perspective.

Bias correction was performed using a modified version of quantile matching. While quantile matching (Déqué, 2007) has seen successful application in coastal modelling settings (Parker et al., 2017), this study has a much larger region of interest

where exact matching of model cumulative distribution functions (CDFs) to observations becomes problematic. Specifically, applying corrections derived at tide gauges to locations far from the tide gauge may introduce errors. While this approach is possible, most likely through interpolating corrections between tide gauges, it is likely that an exact CDF matching constraint is too strong and may result in overfitting. For example, there is no reason to assume that the GTSM-ERA5 bias measured at a tide gauge located deep within a hydraulically complex river mouth is the same as the bias at a nearby ocean coast location. This study compares each tide gauge to GTSM-ERA5 data as a single sample of the overall error in the model. We therefore correct the GTSM-ERA5 data at each quantile by the average error across all tide gauges. The same correction (based on the average error) is applied across the entire region, as shown in Figure 4.

330

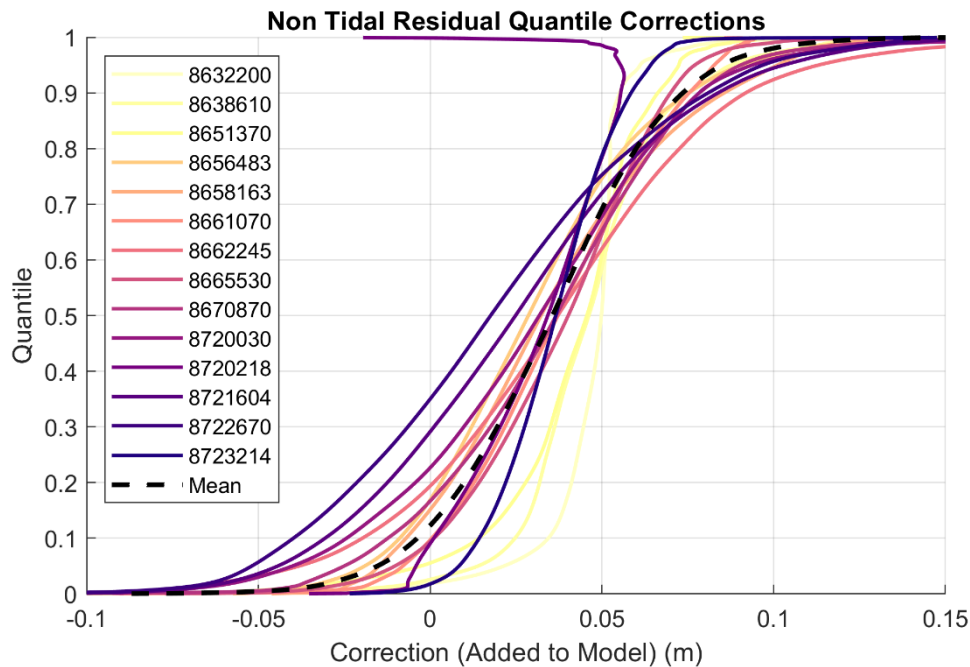


Figure 4: Visual representation of the utilized quantile-based statistical correction for non-tidal residuals. Each line represents the Cumulative Distribution Function (CDF) corrections to fit modelled CDFs to observations at individual tide gauges. The dotted line is the applied correction representing the average quantile correction across all gauges.

335

This figure plots the difference (observed NTR – modelled NTR) between CDFs at each quantile. Therefore, the value on the x-axis (correction) is the amount that must be added to the model NTR to exactly match the observed CDF. The dotted line is the average of all tide gauges and therefore the correction applied to the GTSM-ERA5 NTR data across the entire region. Figure 4 shows that GTSM-ERA5, in general, overpredicts low NTR and underpredicts high NTR (a bias towards too little variability). The median bias (quantile 0.5) is low (model underprediction) and this low bias increases moving towards larger

340

NTR with the largest underpredictions found for the upper extreme NTR. Across tide gauges, the general trend, although with significant variability, is increasing bias in NTR moving from the South (Darker colors) to the North (Lighter colors).

Notably, three outlier gauges were removed from this analysis and not included in the average correction calculation. Tide gauges 8652587 (Oregon Inlet, NC), 8654467 (Hatteras, NC), and 863901 (Chesapeake Channel, VA) correction CDFs were found to deviate significantly from the general pattern shown in Figure 4. Gauges 8652587 (Oregon Inlet, NC) and 8654467 (Hatteras, NC) were highlighted earlier in section as likely effected by a mesh resolution / bathymetry related issue. Gauge 8638901's (Chesapeake Channel, VA) outlier behaviour is probably due to an insufficient overlap between the GTSM-ERA5 and tide gauge record (less than a year). Additionally, the gauge is located at the center of the Chesapeake Bay inlet and likely experiences complex hydrodynamics not resolved by GTSM-ERA5. Based on these arguments, it was judged valid to remove these outlier stations from the NTR statistical correction procedure.

3.2 Wave Setup

This study additionally considers waves as an important driver of coastal MWLs in the study region (Dietrich et al., 2011a, 2011b). The primary pathway through which waves influence flooding is wave setup, via an increase in mean sea level near the shoreline caused by the transfer of momentum during wave breaking. While either wave run-up or setup could have been considered in this study, wave setup was selected because sustained flooding occurs at timescales of hours to days. Wave run-up occurs at scales of seconds to minutes and so wave setup is more influential and appropriate for consideration in a flood hazard case. Waves can additionally affect MWLs through coupling with surge, tides, sea level, and other processes, but these effects are generally smaller than wave setup along the open coast (Idier et al., 2019). There are two approaches for calculating wave setup: physical modelling or empirical formulations. At the scale of this study, 1000s of kilometers, a physical model capable of accurately resolving wave setup would be computationally prohibitive. Instead, this study utilizes the empirical Stockdon formulation (Stockdon et al., 2007), following other large spatial scale approaches (e.g., Melet et al., 2018; Kirezci et al., 2020; Wahl et al., 2016; Serafin et al., 2017).

The Stockdon formulation relates setup at the shoreline to the deep-water wave height, period, and beach foreshore slope. Foreshore beach slope data were obtained from the USGS National Assessment of Coastal Change Hazards (Doran et al., 2020; Kratzmann et al., 2017). The dataset consists of foreshore slopes along pre-defined transects spaced approximately 50 m in the alongshore direction (Farris et al., 2018). Transects were resampled from 50-m spacing to 1-km spacing alongshore. At each transect, a temporally average foreshore beach slope was calculated from all available shoreline data and spatially smoothed using a Hanning filter to minimize noise (Doran et al., 2015). Wave characteristics were determined by extracting data from the full ERA5 (Hersbach et al., 2018; Hersbach et al., 2020) wave output grids along the 10 m depth contour. ERA5 wave data were then matched to the nearest transect offshore endpoint, while also preventing duplication with multiple wave data points matched to a single transect location. The 10 m depth ERA5 wave data were then reverse-shoaled to respective deep-water conditions using linear wave theory and assuming a shore-normal approach. This approach, rather than directly extracting the wave parameters from deep-water, was taken for two reasons. The first was to account for local changes to wave

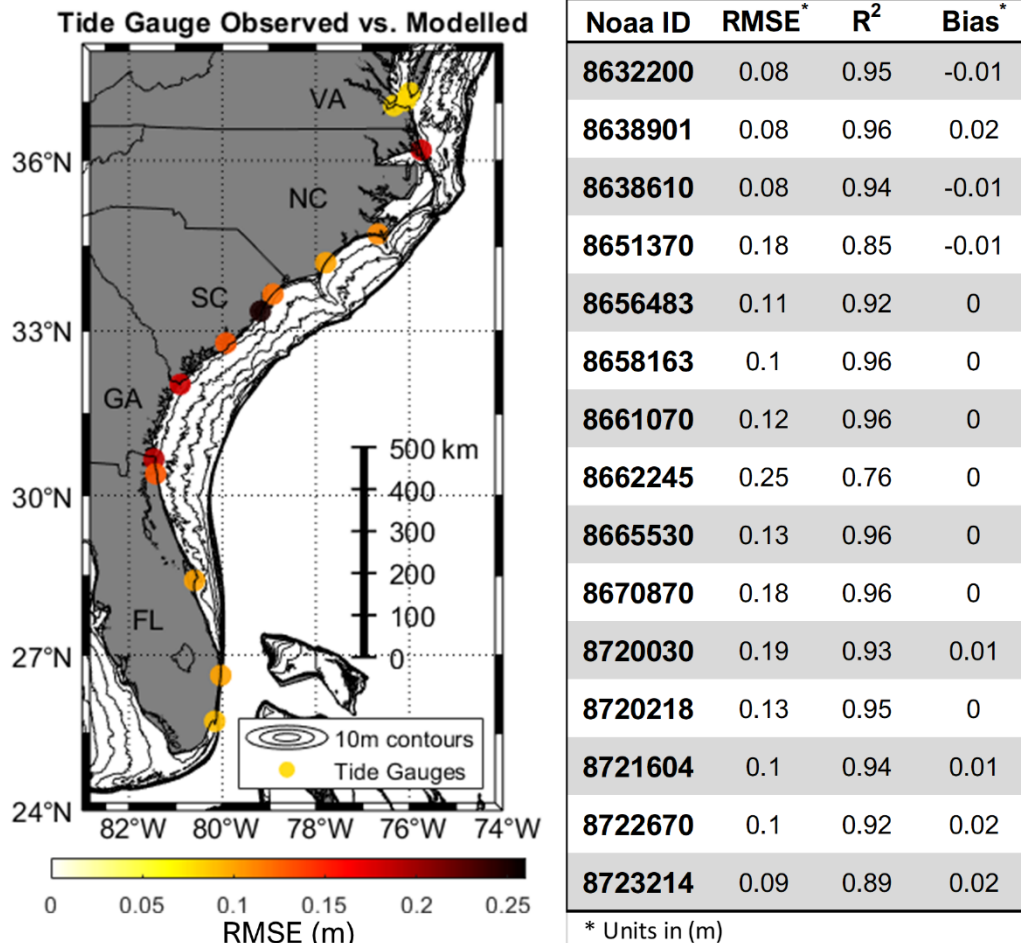
conditions between deep-water and the nearshore. The second was for consistency with the methodology used in developing
375 the wave setup parameterization, e.g., Stockdon et al. (2007). The spatial resolution of the transect based wave setup data are
significantly finer than the GTSM-ERA5 data. Therefore, a characteristic setup was calculated for each GTSM-ERA5 data
location by averaging wave setup across all transects within 5 km of the location of interest. It is also worth noting that the
utilized wave setup parameterizations predict wave setup at the beach while GTSM-ERA5 output stations are in the nearshore.
There is therefore a cross-shore offset between these two MWL components. This was explored further by examining GTSM-
380 ERA5 output stations located at multiple locations in the cross-shore to see how much predicted SWL varied. No significant
difference was found, so the cross-shore offset was deemed to be similarly nonrelevant to results. This conclusion is likely
since the processes responsible for changes to MWL in the nearshore (e.g., wave setup/setdown, three-dimensional circulation,
etc.) are not resolved in the GTSM-ERA5 model.

4. Model-Observation comparisons.

385 Assessment of model improvements following individual SWL component corrections was evaluated by comparing
observed and modelled timeseries data (Barnard et al, In Review) at each of the tide stations. Model performance was validated
both from a SWL perspective, but also for individual contributing signals. This section starts with an evaluation of SWL and
then evaluates model-observations differences of each contributing component described in the preceding sections.

4.1 Water Levels

390 Figure 5 shows both a visual and table-based comparison of observed and modelled SWLs (corrected) at all tide
gauges within the region. As for comparisons above, Station 8652587 and 8654467 (Oregon Inlet, NC, and Hatteras, NC) were
removed as unresolved by the model. Calculated skill values are for the full overlapping period between the tide gauge record
and the SWL hindcast.



395

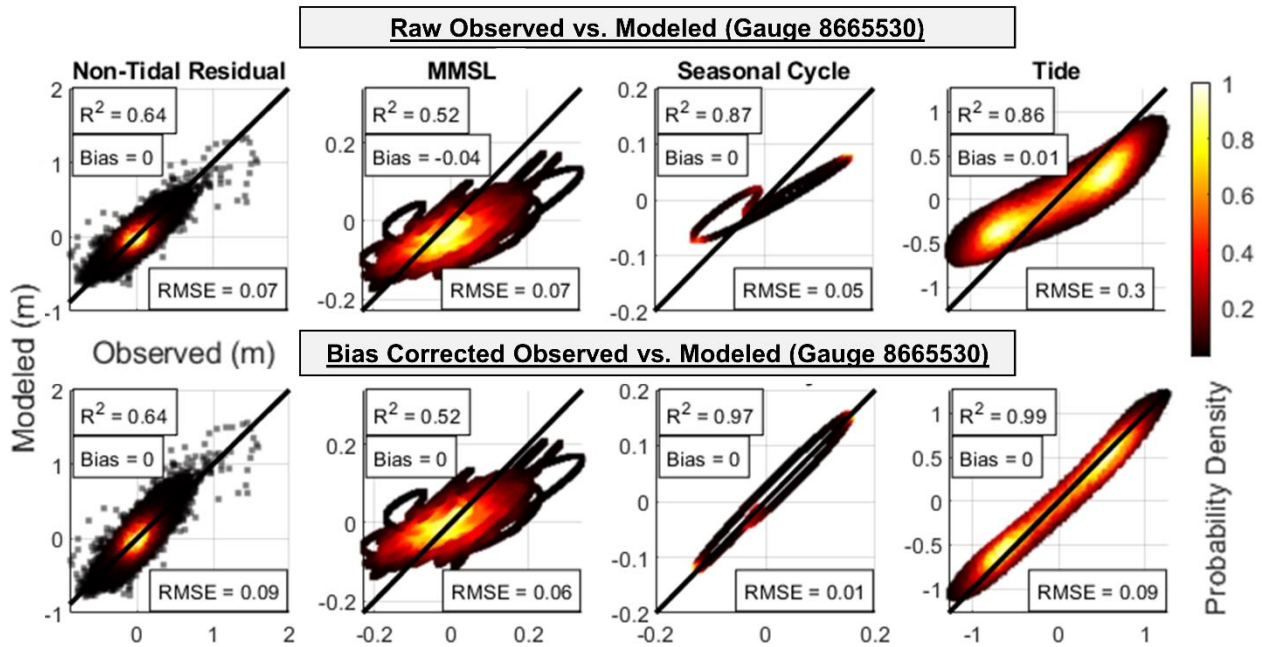
Figure 5: Model skill comparison between corrected GTSM-ERA5 SWLs and tide gauge data. The left panel shows the data spatially by plotting RMSE at the location of the utilized tide gauge. The right panel shows the model skill data in table format.

Overall, it is found that SWLs are well predicted by the corrected GTSM-ERA5 data. The calculated RMSE from the overall modelling framework is comparable with other studies / models using much more complex and finely resolved models. In addition to improvements of RMSE, overall bias in the model is reduced to below 2 cm for all gauges.

4.2 SWL Component Signals

Signal decomposition both provides the opportunity for process specific corrections, but also to examine model performance for different SWL components. Figure 6 shows a comparison of GTSM-ERA5 model outputs versus observations at a single tide gauge: 8665530 (Charleston, SC). This location was chosen for its average performance across the various

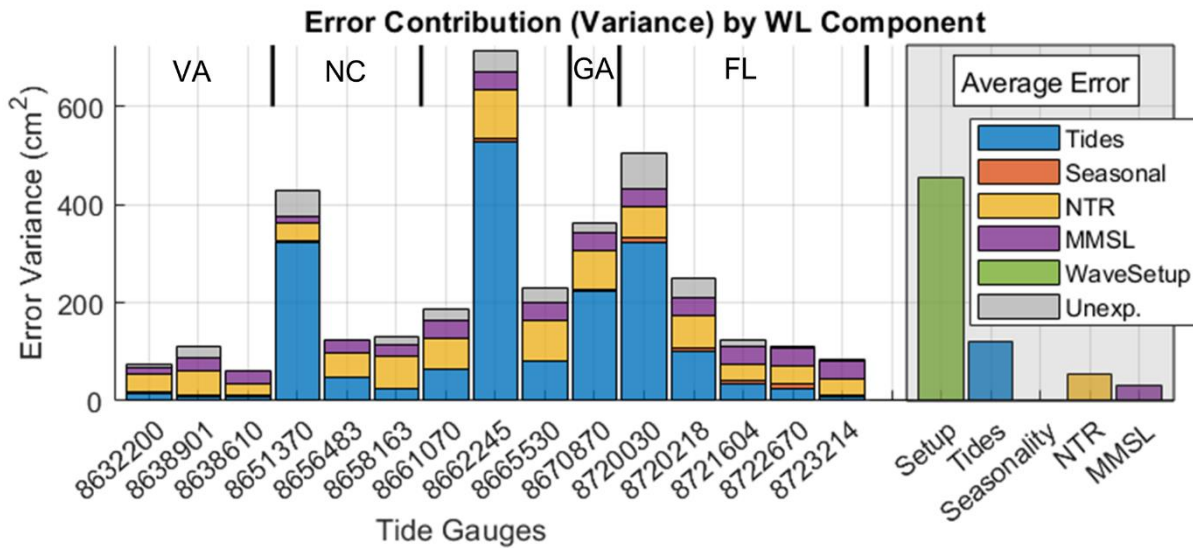
SWL components as well as being located near the center of the study region. Figure 6 shows the effects of statistical correction by including model performance both for the raw (top row) and Bias Corrected (bottom row) GTSM model output.



410 **Figure 6: Observed versus model scatter plot for Non-Tidal Residual (column 1), MMSL (column 2), Seasonal Cycle (column 3), and Tide (column 4). Row 1 corresponds to the raw data from GTSM-ERA5 while the 2nd row corresponds to the model results after statistical correction. Data are plotted for NOAA tide gauge 8665530 (Charleston, SC). The plotted scatter color is based on the density of points in the region with dark colors being less dense and light colors being denser.**

415 In Figure 6, the most noticeable changes are for the seasonal and tide corrections with large improvements to RMSE and model skill. For this specific tide gauge, NTR corrections did not improve overall/average NTR. Extreme NTRs were found to be improved which can be seen by the shifting of higher NTR datapoints. MMSL scatter shape is not changed, due to the nature of the correction, but the bias is removed via a vertical shifting.

To further understand inter-station variability in model performance, an analysis was performed to determine each
 420 MWL component's contribution to MWL error. For this analysis, the RMSE (which is the same as the standard deviation of the error) is converted to variance. This is because variances are additive (assuming independence), allowing us to sum the errors of individual components. Therefore, theoretically the variance of each MWL component should add up to the variance of MWL. This is mostly true with a small amount of "unexplained" variance (marked in Figure 7 in grey) that is due to the components not being truly independent.



425

430 **Figure 7: Error variance between the observed and model SWL at each tide gauge location and separated by process signal. Unexplained variance is the difference between the total error variance and the sum of the individual components. Top brackets show the state where each tide gauge is located. The final “Average Error” section shows the average error variance across all tide gauges as well as an estimate of the error variance for wave setup (not calculated at each tide gauge station) from Stockdon et al. (2007).**

From Figure 7, poorly performing locations are traced to the source SWL component. Tides are the main source of poor SWL predictive skill, with error an order of magnitude greater than the other components at stations 8651370 (Duck, NC), 8662245 (Oyster Landing, SC), 8670870 (Fort Pulaski, GA), and 8720030 (Fernandina Beach, FL). Therefore, improvements to the tide model at poorly performing locations is the most viable way to improve overall model performance. Seasonality is a non-relevant contributor to error while NTR and MMSL are approximately uniform across station locations.

440 A general estimate of wave setup error is plotted as the far-right bar in Figure 7 for comparison to other SWL signals. This estimate was based on the regression RMSE from Stockdon et al. (2007). Station explicit setup error estimates are not included because no data exist for wave setup at tide gauges. Furthermore, tide gauges are generally considered to not contain wave setup signals. This is not because wave setup is absent in locations with tide gauges, but rather that the mechanics and signal processing of tide gauges is designed to filter out wave setup signals (Sweet et al., 2015). Therefore, wave setup is considered absent in both the observations and modelled datasets, so not included in the statistical correction. With no observed data for comparison, as well as reduced physics (parameterization vs. a physical model), wave setup can be considered to have a relatively high level of uncertainty. This is reflected in the large, plotted error variance in Figure 7, which is more than double the SWL error at most tide gauge stations.

4.2.1 Tides

Tides were found to be the largest source of error in uncorrected GTSM-ERA5. This is in part because tides are the dominant source of SWL variability in the region. Therefore, small errors in phase or amplitude of tidal constituents can control the overall error in a SWL comparison. Also, GTSM-ERA5 is a purely hydrodynamic model with tides generated internally. While global scale hydrodynamic models have made significant recent progress (Apecechea et al., 2017), they remain less skillful than data assimilation-based products (Stammer et al., 2014). Table 1 confirms this via comparison to tide gauges and strengthens the decision to use the ensemble tide method.

For the ensemble, the resulting tidal data are better than any of the contributing tidal models, although only by a small margin (see Table 1). This said, the tidal ensemble has other intrinsic benefits such as uncertainty estimation and an efficient pathway to include additional tidal information as it becomes available. Additionally, it is likely that improvements to the tidal ensemble could be made by including more tide models, better tuning of the weighting function (eqn. 2) or incorporating corrections.

As noted above (section 4.2 and Figure 7), tides dominate the model error at some of the tide gauges (gauges 8651370, 8662245, 8720030, 8670870: Duck, NC, Oyster Landing, SC, Fernandina Beach, FL, Fort Pulaski, GA). In general, at these locations none of tide models successfully reproduce the tidal signal. Tides are handled fundamentally different in this study than the other components of SWL in that the methodology uses ensemble methods to produce a better tide estimate, rather than a statistical correction. Because observations are not used for corrections (only in the weighting), if all models in the ensemble agree about an incorrect tidal signal, then the ensemble calculated tides will similarly be incorrect. Tide gauges 8662245 (Oyster Landing, SC) and 8720030 (Fernandina Beach, FL) are both located within complicated estuary systems where local complexities of tidal wave propagation are likely not being fully resolved by the utilized coarse scale global tide models. This resolution issue is likely less of an issue at the open coast locations used for analysis in this study.

4.2.2 Seasonality

The seasonality correction was found to greatly improve the seasonal signal. Overall RMSE (across all gauges) was reduced from approximately 5 to 1.5 cm through the correction. From the average perspective, the correction is found to work well, but with an overcorrection at the farthest north gauges (8632200, 8638610, and 8651370; Kiptopeke, VA, Sewells Point, VA, Duck, NC). Even for these “overcorrection” sites, corrected seasonality was found to make up the smallest fraction of the error budget (see Figure 7). Based on this analysis, a more complicated correction was decided to be unwarranted.

4.2.3 Monthly Mean Sea Level

Corrected MMSL values reasonably match observed values. Figure 6 shows that MMSL skill (as measured by R^2) is less than for other SWL components. This is because MMSL is subject to less stringent corrections than other components. GTSM-ERA5 MMSL was found to be sufficiently accurate that more complex statistical correction was not warranted. This

said, Figure 7 shows that MMSL can become a proportionally larger percentage of the overall error if overall error is small. For example, at station 8723214 (Virginia Key, FL) MMSL represents approximately half of the overall error. As this study is most interested in overall error in predicted SWL, this is not problematic as the overall error remains low. GTSM-ERA5's ability to reproduce MMSL was unexpected based off previous research showing the importance of the Florida Current (Ezer et al., 2013), which should be unresolved in a two-dimensional (2D) hydrodynamic model implementation.

4.2.4 Non-Tidal Residual

For the study region, NTR is the second largest contributor to SWL, and often the largest contributor during extreme events. Therefore, a proper handling of NTR in the modelling framework is requisite for properly resolving flooding and coastal hazards. After correction, GTSM-ERA5 NTR data match observations (average RMSE of 7 cm). NTR performance varies location to location (around 5 cm), likely due to the individual bathymetry characteristics of the tide gauge locations. For example, the worst performing comparison (station 8662245, Oyster, Landing, SC) is located in a complex shallow estuary, far landward up a small braided tidal channel. The utilized resolution for producing the GTSM-ERA5 dataset is unlikely to properly resolve NTR propagation up an estuary of this type.

5. Extreme Values and Relevant Drivers

This study represents a large temporal and spatial hindcast of MWLs that are relevant for a variety of users and applications. Significant efforts have been made to apply robust corrections and improve overall model skill through iterative validation. Results presented in this section will focus on MWL extremes as the primary driver of coastal flooding. Extreme events are defined in this section using the Point-Over-Threshold (POT) method with de-clustering of events to prevent the double counting of individual storm events (Wahl et al., 2017). A unique POT threshold value is selected for each GTSM-ERA5 station. The utilized threshold is calculated using an iterative procedure that sets the threshold using the constraint that a specified number of extreme events are selected out of the full record. Extreme values are calculated from the MWL timeseries consisting of both the GTSM-ERA5 derived SWL and the wave setup components. The following sections also discuss empirical recurrence interval events, which are calculated by ranking the POT events and inverting the empirical CDF. Using this definition, the annual event is the 38th largest POT event out of the 38-year record and the maximum observed event has a 38-year recurrence interval.

5.1 Contributors to Extreme MWLs

Figure 8 shows GTSM-ERA5 output for all stations and all water level components along the study region coastline. The data are presented in two ways to demonstrate how contributions vary spatially (panel b) and how contributions are a function of event rank (panel c).

Component Contributions to Extreme Water Levels

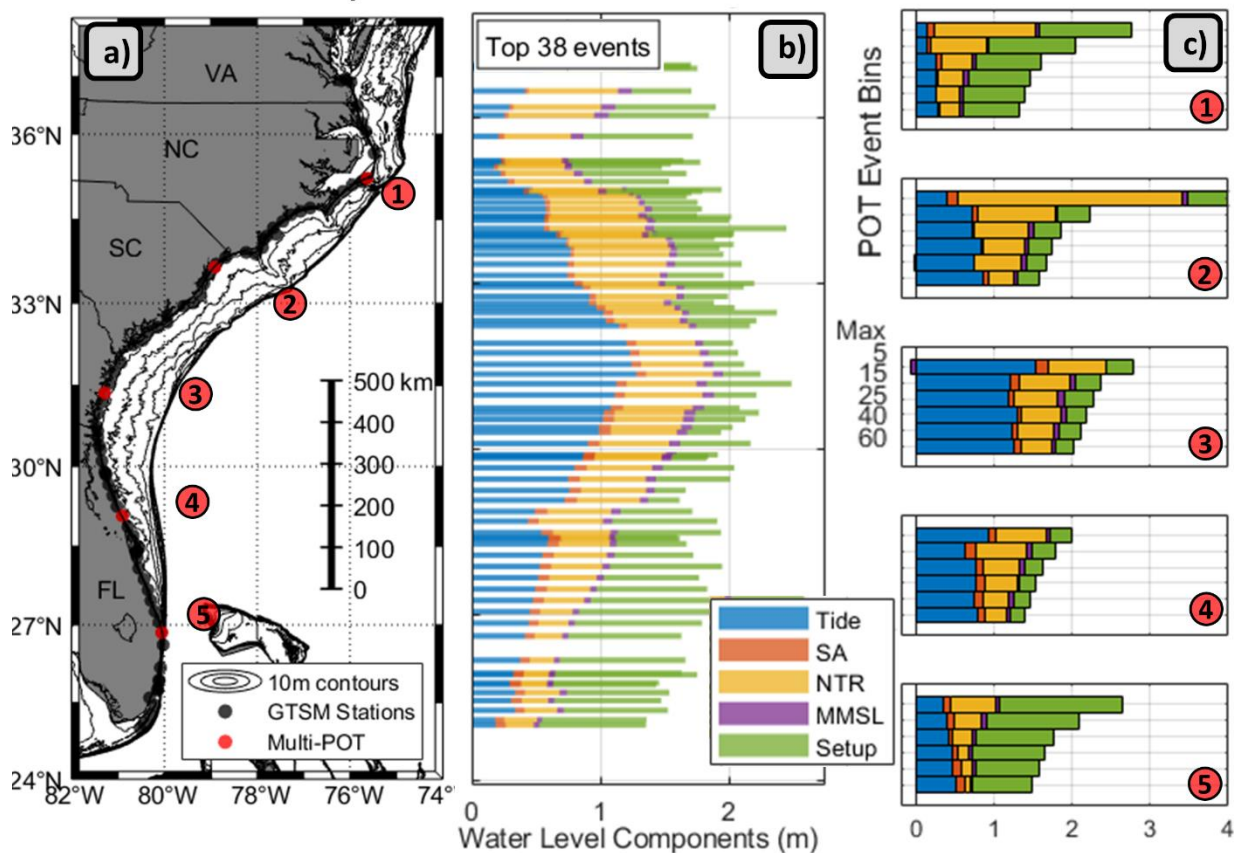


Figure 8: Panel a) shows GTSM-ERA5 stations (in black) with highlighted “multi-POT” node locations marked in red and numbered to correspond with panel c). Panel b) shows the average contribution to MWLs for the top 38 events (equal to the number of simulated years) at each station. Panel c) shows the contribution to extreme MWLs for the max event (top bar) and binned events ranging from 5th largest to 60th largest. Binned values are calculated by averaging the 10 events bracketing the event rank of interest (e.g., the plotted bar for rank “15” is the average of all events from rank 10 to 20).

510

Extreme events are both compound (composed of multiple signals) and variable along the coastline (Figure 8). Tides, NTR, and wave setup are the dominant contributors to extremes with the balance between these signals varying as a function of latitude. The average contributions for the top 38 events (approximately the 1-year event to the 38-year event: panel b) show that the tidal component displays the most spatial variability. Tides are most important at the center of the study site, around Georgia and South Carolina, with the relative magnitude tapering to the north and south. Tidal range in general is larger in this region with the coastline sweeping landward away from the nearest amphidromic point. Wave Setup has the opposite spatial pattern as tides, reaching a minimum at the center of the study region and increasing moving north and south. NTR is more spatially uniform, although a general trend is present with NTR decreasing moving south. The sum of the components follows a spatial pattern similar to tides, reaching a max near 31 degrees latitude and decreasing moving north and south.

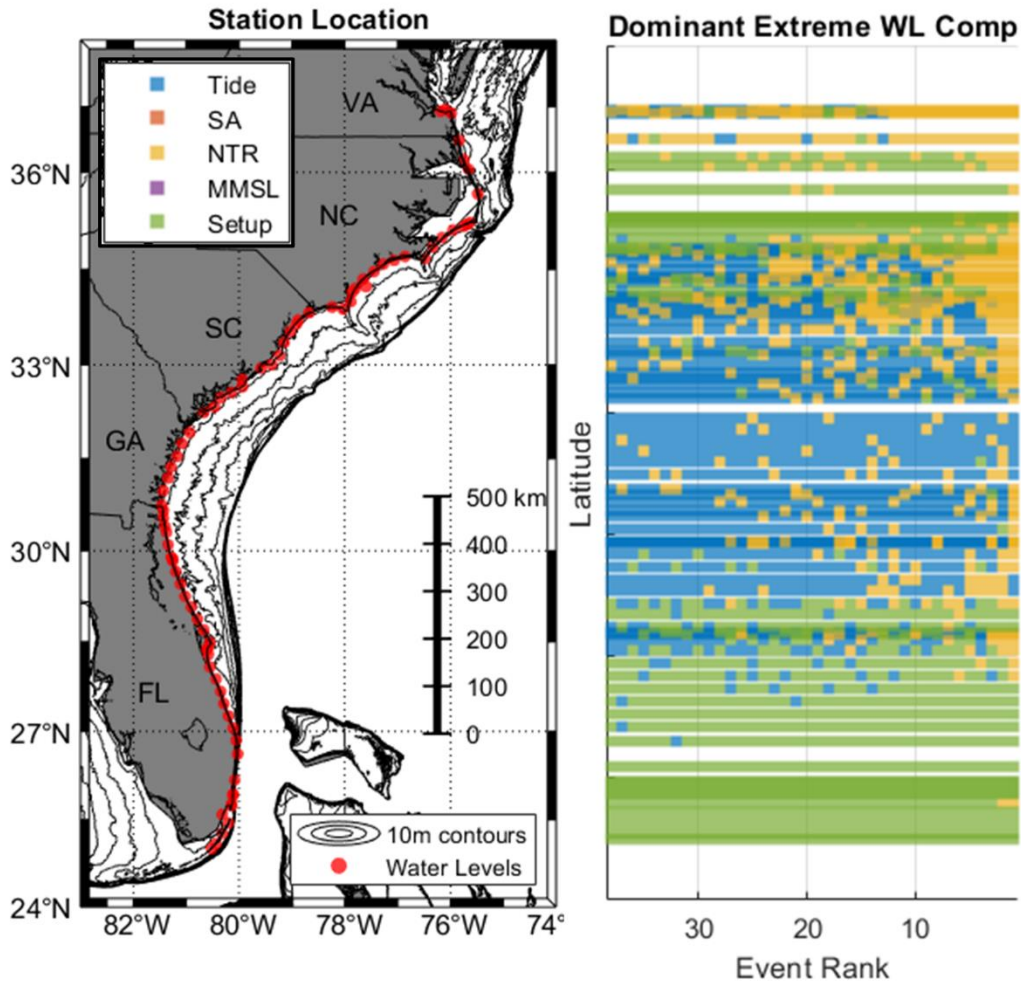
520

Panel c of Figure 8 shows how contributions to extreme MWLs change as a function of event rank. Rather than looking at individual events of a certain rank, plotted is a binned value calculated by averaging the 10 events bracketing the event rank of interest. Therefore, the plotted bar for rank “15” is the average of all events from rank 10 to 20. Binning is done to provide a more robust interpretation of MWL contributions that smooths over event-to-event variability. The plotted “max” event is an exception, which is not binned but still included to show the most extreme hindcasted event. In general, the NTR contribution increases moving from the 60-bin rank (bottom bar in each subplot) to the max event (top bar in each subplot). This is especially visible in subplot 2, a location near the border of North and South Carolina. At this location, NTR magnitude more than triples moving from the rank 60 bin to the max event. Tides are found to be more uniform in magnitude, which is expected due to the random nature of the co-occurrence of storms and tides. Tidal contributions may vary from event to event but would be expected to have a somewhat consistent contribution when averaged across multiple events. The wave setup contribution increases slightly moving from more frequent events to the most extreme.

Results also show that the location of maximum event magnitude along the coast is dependent on the recurrence interval of the event considered. The average of the top 38 events, Subpanel b, has a spatial maximum at around 31 degrees latitude. The maximum event, on the other hand (shown in subplot c as the top bar), is much larger at 34 degrees latitude. This suggests that different locations are more susceptible to nuisance level flooding while others may be more susceptible to higher recurrence interval (rare) events. That said, the large difference between the Rank 1 and Rank 2 events (not shown) in the region around 34 degrees latitude suggests that the hindcasted extreme event may be uncharacteristically extreme. A larger sample of storms would be necessary to properly constrain the magnitude of the 38-year recurrence interval storm.

5.2 Dominant Forcing Mechanism for Extreme MWLs.

Of interest to coastal hazard analysis is the specific process that is the “dominant” contributor to extremes. This allows for a conceptual understanding of what processes are important and the types of events that need to be considered. For example, coastal risk mitigation strategies will likely be different if flooding is controlled by tides or hurricanes. This concept is further explored for the study region in Figure 9.

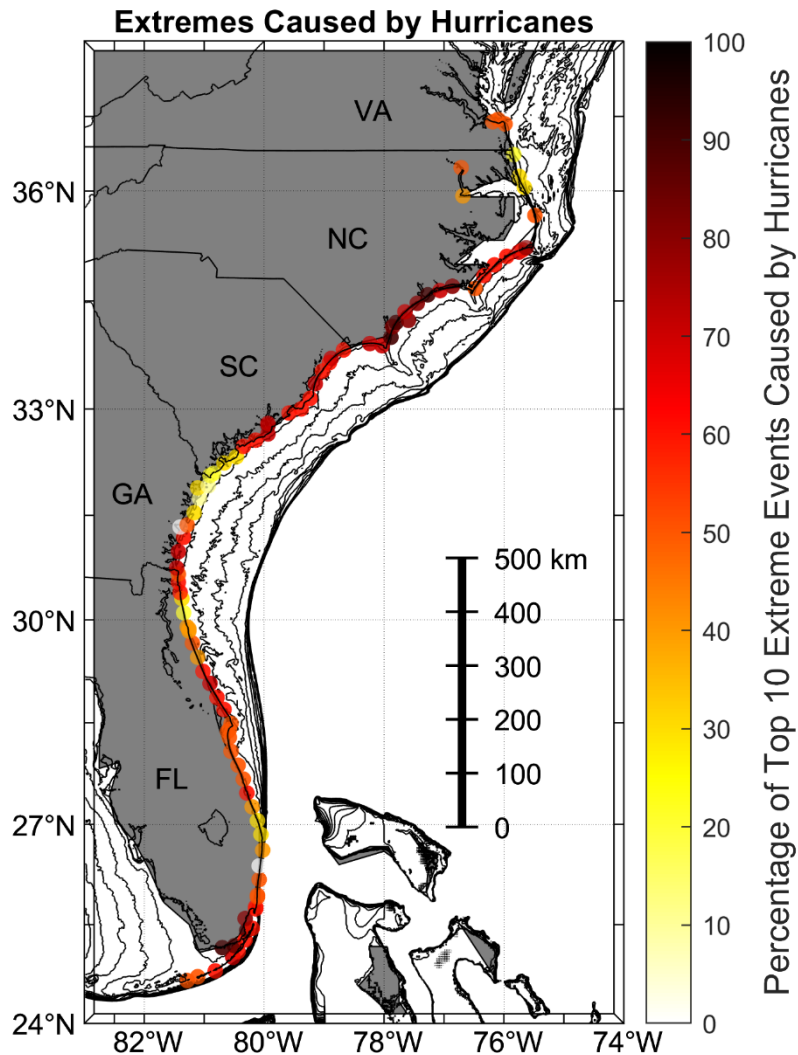


550 **Figure 9: Dominant MWL component for the top 38 ranked events at each GTSM-ERA5 station. The first panel plots the GTSM-ERA5 output stations which have their dominant components plotted in the second panel. For the second panel, each row represents a GTSM-ERA5 output station, and each column represent an extreme event, with event rank 1 being the highest over the 38-year record. The color indicates what MWL component was dominant for the specific ranked event.**

Figure 9 plots the dominant MWL component for each individual event ranging from the 38th largest event (Annual event: left side of the plot) to the largest event (38-year event: right side of the plot). Event rank is determined at each station, so columns do not necessarily represent a temporally consistent event. This plot differs from Figure 8 in that MWL contributions are not averaged/binned, so the individual variability between events can be seen. This shows that many stations have a mixture of dominant event contributors, often sharing between tides, NTR, and wave setup. Therefore, no location has a “standard” MWL component mixture that could simplify the modelling process. This said, in general, setup is found to be more dominant in the south, tides in the central region, and NTR in the north.

Both Figure 8 and Figure 9 bring to focus the importance of NTR for the most extreme events. Tides, MMSL, seasonality and wave setup (to a lesser degree) are bounded while NTR has the potential to become very large. Large NTR signals are shown by the top bars in Figure 8, panel c (max observed event), as well as NTR being more often dominant moving towards more extreme events in Figure 9. Large NTR signals are primarily the result of hurricanes which can drive surge on the scale of meters (Irish et al., 2008; Woodworth et al., 2019). For this reason, many studies only consider hurricanes in hazard assessments as these events are considered the primary cause of extremes (Marsooli et al., 2018). Figure 9 shows this assumption is not strictly valid since some locations are not NTR dominated (e.g., southern Florida, where a narrow shelf limits storm surge), even for the max observed event. Moving towards less extreme events, this assumption become increasingly weaker, with the annual event (rank 38) being almost entirely dominated by signals other than NTR.

While hurricanes are in general characterized by large NTR signals, it is possible that hurricanes are still driving extremes even if NTR is not the dominant signal. Figure 10 explores this concept further by plotting the percentage of the top 10 extreme events produced by hurricanes along the study region. This was determined by selecting the top ten ranked events at each location and then cross referencing their occurrence date with a database of hurricane arrivals along the coast. The extreme MWL event was considered to be caused by a hurricane if the MWL event was within 2 days and 500 km of hurricane land arrival.



575 **Figure 10: Percentage of top 10 extreme events that can be traced to local hurricane forcing.**

Figure 10 shows that for much of the region, hurricanes are major drivers for extreme events but not the only driver. For many locations, only half or less of the top 10 events are related to a hurricane. Therefore, only modelling hurricanes would miss a significant number of extreme events and bias the resulting extreme value analysis. The Mid-Northern part of the study region is more effected by hurricanes with up to 100% of the top 10 events being hurricane driven. The large number of hurricanes is contrasted by parts of the middle of the region (near Georgia) where closer to 3 of the top 10 extreme events are related to hurricanes. Notably, this does not signify that these areas were not impacted by hurricanes, just that the result was not necessarily a top 10 extreme event. The presence of non-hurricane top 10 events emphasizes the importance of the co-occurrence of various signals (e.g., high tides, large waves, etc.) to produce an extreme event. Furthermore, this shows that

585 using only hurricane events to constrain the recurrence interval of extremes is likely missing many of the most extreme events, even up to the 38-year event. The record length of this analysis (38 years) is a limitation to the robustness of this conclusion, which is explored further in the discussion (section 6.3).

6. Discussion

6.1 Model Performance for SWL components

590 Overall, the modelling framework detailed in this study is found to perform quite well for predicting SWLs, exhibiting a similar skill to significantly more finely resolved or physically complex models. For example, Olabarrieta et al. (2011) produced RMSEs of the same order using the fully wave coupled three-dimensional (3D) COAWST model implemented with 75 m grid resolution. Also, this study's model-observation comparisons are done against tide gauge data, which are most often located within ports or estuaries. Therefore, the observation points used for comparison are not a proper sample of the full
595 study region and likely provide a non-representative interpretation of GTSM-ERA5's skill as developed in this study. It is expected that GTSM-ERA5, which serves as the basis for MWL calculations, would perform better at locations with less complex and fine-scale bathymetry. GTSM-ERA5 output stations used for analysis and the hindcast product are all at open coast locations, away from the complex geometries and hydrodynamics of inlets. Therefore, the presented model skill analysis is likely a conservative estimate of the overall model skill.

600 As a potential source of error, Delft3D FM does not provide output at specified locations exactly (either through interpolation or direct calculation) but rather snaps output to the nearest mesh node location. Therefore, GTSM-ERA5's produced output can be from a location spatially offset from the actual tide gauge. Based on mesh resolution, this shift is a maximum of around 1 km. As, in general, surge and tide signals are slowly varying, it is expected that the effect of this potential mismatch in locations is minimal, and that accurate representation of shoreline boundaries and depth variations contribute
605 more to the differing results. However, this spatial shifting could have more of an effect in complex bathymetric regions.

An additional consideration in model performance is that NTR was found to have a large amount of high frequency variability. Both the observed and modelled NTR timeseries are found to be "noisy" with a large amount of energy with a frequency >0.007 Hz (1/6 hour). Analysis showed that there is no statistically significant correlation between GTSM-ERA5 and observed NTR for this high frequency NTR. It is possible that this high frequency energy represents locally controlled
610 NTR (either by fine scale bathymetry or local forcing) which is below GTSM-ERA5's resolution. This noise could also be an artifact of how NTR is being calculated. Interaction between surge and tide can create lags between the tidal and full SWL timeseries. The subsequent subtracting of the two timeseries can then produce spurious NTR signals (Horsburgh et al., 2007). As a sensitivity study, the NTR statistical correction framework was run with the high frequency NTR signal removed (taking the assumption that high frequency energy is white noise). This procedure was found to produce a lower NTR RMSE, but it
615 was decided to not take this approach because real NTR signals can exist within this high frequency band. For example, it was found that the removal of high frequency energy was smoothing out /removing NTR pulses from hurricanes, which can happen

at small timescales. Secondly, it was decided to not remove the high frequency noise as a potentially misleading assessment of true RMSE. With a fair bit of the model error residing in high frequency noise, assessment of model skill with this signal removed may represent a false metric of actual model performance.

620 **6.2 Model Performance for extreme SWLs**

With this study's focus on extreme events, it is worth considering model performance specifically for extreme events. An analysis based on 50 extreme events for each location shows that overall (across all tide gauges) RMSE for predicted SWL increases from 13 to 18 cm. The bulk of this increased error is due to NTR. NTR RMSE approximately doubles from around 7 to 12 cm when looking at only extremes. In addition to NTR, MMSL RMSE increases by 2 cm. Both tides and seasonality
625 show no change in model error. This is because storm arrival is approximately random in time and so no more likely to occur at a specific tide or seasonal phase. In other words, tide and seasonality error is approximately uniform in time so not affected by when extremes occur.

The decrease in model performance for extreme SWL is expected as, in general, extremes are more difficult to model. Current hydrodynamic models tend to underpredict extreme surge events for a variety of reasons ranging from wind fields
630 (Akbar et al., 2017) (which are often the leading cause) to the utilized physics implementation (Weisberg and Zheng, 2008) to model resolution. Additionally, this study's choice of modelled processes is missing some physics that may be contributing to error, such as surge/wave interactions (Idier et al., 2019) and 3D effects. GTSM-ERA5 was produced using the 2D barotropic version of the Delft3D Flexible Mesh model. While baroclinic processes have been shown to be important at specific locations within the study region, implementing a global baroclinic model would be computationally prohibitive while only improving
635 model skill on the order of 1-2 cm (Ye et al., 2020). Overall, the calculated model skill is found to be in alignment with the current state of the practice for surge modelling. As a comparison point, Marsooli et al. (2018) used coupled ADCIRC / SWAN to predict maximum hurricane surges within the same study region. Model validation for this alternative methodology showed a RMSE of ~20 cm on average. Veeramony et al. (2017) showed an even larger average RMSE of ~40 cm using Delft3D to simulate Hurricane Ike. Therefore, this study's utilized modelling strategy is consistent, in terms of model skill, with the current
640 state of the practice.

6.3 Contributing Signals to Extreme MWLs

This study emphasizes the importance of compound flooding, with all three of NTR, tides, and setup being important for properly modelling extreme MWL along the coastline. Seasonal and MMSL signals were found to be smaller contributors to extreme water levels. However their magnitude and coincidence with the other components still make them important for
645 hazard analyses, especially when considering less-extreme events. The compound composition of water levels in this region means that timing and co-occurrence is important for an extreme event. Even an extremely large NTR event is unlikely to produce an extreme event if it arrives on a low tide. This agrees with previous research that has emphasized a proper handling

of the co-occurrence of forcing parameters for modelling extreme events (Wahl et al., 2011) rather than more simplified approaches such as considering the max surge added to a maximum tide signal.

650 This study further emphasizes other recent research highlighting the importance of wave setup as a contributor to extreme MWL (Melet et al., 2018; Ruggiero et al., 2013). At the national scale, setup has been found to contribute 10-82% of water levels during extreme events (Vitousek et al., 2017, Sweet et al., 2022). Setup was found to be more often the dominant component in the southern region of the study site. Setup variability is likely because the U.S. Atlantic coastline is characterized by a broad continental shelf which limits the amount of wave energy that can penetrate to the coastline (Defne et al., 2009).
655 The southern region of Florida has a much smaller continental shelf (see depth contours in Figure 8 or Figure 9), allowing more wave propagation and therefore a larger wave setup along the coast. Wave setup has significantly more uncertainty than other modelled MWL signals in this study. Setup data for specific events should be treated as an order of magnitude estimate rather than an exact calculation. Since there is no reason to suspect any systematic bias in wave setup parameterizations, it is expected that aggregated average values for setup contributions should be more robust.

660 This study takes the pragmatic approach of only discussing events within the hindcast period and does not extrapolate to larger return period events. This study's hindcast period of 38 years only contains the observed number of hurricanes and storms, so is vulnerable to uncertainty from non-observed variability in storms and MWL components (Serafin and Ruggiero, 2014; Lin and Emanuel, 2012). This study avoids extreme water level value analysis beyond the modelled 38 years, which would amplify uncertainty. Additionally, readers should consider analysis based on the most extreme event of the record (e.g.,
665 Rank 1 in Figure 8) as less certain than the averaged results containing multiple samples. An example of how this effect is the lack of hurricanes within the extreme record for the center of the region (Figure 10). Hurricanes are less common in this area (Bossak et al., 2014), but the rare direct hurricane hit is still possible. This direct hit would produce a very different MWL composition (likely more NTR dominated). It is impossible to determine exactly how rare this type of event is or how it would affect extreme event composition without simulating a very large number of hurricane events (Lin and Emanuel, 2012). This
670 type of study is outside the scope of this paper; readers are cautioned that presented results are only for the hindcast period and not a general conclusion regarding extremes.

While this study is unable to consider larger recurrence interval events due to an under sampling of storms and an insufficient record length, its continuous timeseries approach is well suited for examining higher frequency extreme events (annual to 15-year recurrence period). Studies which only model hurricane events or specific storm events implicitly assume
675 that those types of events are always responsible for flooding. This is likely true for high return period events but becomes increasingly suspect moving towards the annual event. This study shows that modelling just hurricanes would be insufficient for constraining even the 30-year recurrence period event. While not shown, the maximum event at stations across the region was found to be hurricane induced for only around half of the GTSM-ERA5 output stations during the 38-year time-period from 1979 through 2017. Therefore, an ideal modelling strategy to assess coastal flooding hazards within the region would
680 require blending multiple hurricane/storm simulations (for higher return period events) with a non-hurricane-based compound flooding component (for lower return period events).

7. Conclusions

This study presents a new approach for modelling large scale (both temporal and spatial) mean water levels (MWL)s along the coastline. This method pairs the recent Global Tide and Surge Reanalysis (GTSM-ERA5, Muis et al., 2020) with a process specific statistical correction to model non-tidal residual (NTR) and monthly mean sea levels (MMSLs). Tides are modelled using a novel ensemble technique which combines multiple global tide models to produce an optimal tidal hindcast for the study region. Open coast wave setup data are estimated using a setup parameterization. Based on comparisons to observations at all tide stations within the study region and outside of highly flow constricted water bodies, the resulting hindcast was found to perform well with an average root mean square error (RMSE) of approximately 13 cm. Tides were found to be the largest contributor to error, likely due to insufficient bathymetric resolution in back-barriers and harbors. It is expected that error is smaller at the open coast locations where output stations are placed for the developed MWL hindcast.

The modelling framework is utilized to produce a hindcast of MWLs along the Southeast U.S. Atlantic coastline from 1979 to 2017. An analysis of extremes from this hindcast period found that the contributors to extremes are variable along the coastline. The average tidal contribution to extremes is largest at approximately 31 degrees latitude and then decreases from north to south. Average NTR contributions to extremes increase south to north while average wave setup contributions are the opposite, increasing from north to south. The relative importance of each signal is a function of the magnitude of the event, with larger events in general being more NTR dominated. This said, most locations have a balanced mix of tides, NTR, and setup contributing to extreme events, emphasizing previous research that the co-occurrence of various processes is requisite for extremes. This result is further confirmed in the hindcast, such that not all extremes (even up the 38-year event) are produced by hurricanes. Instead, results show that non-hurricane driven combinations of processes are important to consider for high to mid frequency events (annual to 38-year recurrence interval events).

Statements and Declarations

Competing interests:

The authors have no competing interests to declare that are relevant to the content of this article.

705 Funding

This research/product/data release/tool was funded by the Additional Supplemental Appropriations for Disaster Relief Act of 2019 (H.R. 2157) for North Carolina and South Carolina, and by the USGS Coastal and Marine Hazards and Resources Program for the remaining states. Any use of trade, firm, or product names is for descriptive purposes only and does not imply endorsement by the U.S. Government.

710 **Author contribution**

Kai Parker prepared the manuscript with review and editing contributions from all co-authors. Kai Parker also served as the primary researcher, doing most of the analysis with significant inputs from co-authors. Li Erikson served primarily in a supervision role, but also with significant contributions to methodology and investigation via continual inputs to the study development. Kees Nederhoff contributed to methodology and investigation, providing guidance and assistance on the utilized
715 methodologies as well as interpretation. Jenny Thomas served in a similar role, providing continual contributions to methodology and investigation. Sanne Muis served in a data curation / resources role, providing the base GTSM water level data and expertise in their interpretation. Patrick Barnard served in a project administration, funding acquisition, and supervision role, guiding the overall project from inception to its completion.

720 **References**

- Akbar MK, Kanjanda S, Musinguzi A (2017) Effect of bottom friction, wind drag coefficient, and meteorological forcing in hindcast of Hurricane Rita storm surge using SWAN + ADCIRC model. *J Mar Sci Eng* 5:.
<https://doi.org/10.3390/jmse5030038>
- Andres M, Gawarkiewicz GG, Toole JM (2013) Interannual sea level variability in the western North Atlantic: Regional forcing and remote response. *Geophys Res Lett* 40:5915–5919. <https://doi.org/10.1002/2013GL058013>
- Apecechea MI, Verlaan M, Zijl F, et al (2017) Effects of self-attraction and loading at a regional scale : a test case for the Northwest European Shelf. 1:729–749. <https://doi.org/10.1007/s10236-017-1053-4>
- Armstrong SB, Lazarus ED (2019) Reconstructing patterns of coastal risk in space and time along the US Atlantic coast , 1970 – 2016. 2497–2511
- 730 Barnard PL, Befus K, Danielson JJ, et al (In Review) Future coastal hazards along the U.S. Atlantic coast.
<https://doi.org/10.5066/P9BQQTCI>
- Barnard PL, Befus K, Danielson JJ, et al (In Review) Future coastal hazards along the U.S. North and South Carolina coasts.
<https://doi.org/10.5066/P9W91314>
- 735 Bin O, Poulter B, Dumas CF, Whitehead JC (2011) MEASURING THE IMPACT OF SEA-LEVEL RISE ON COASTAL REAL ESTATE : A HEDONIC PROPERTY MODEL APPROACH. 51:751–767. <https://doi.org/10.1111/j.1467-9787.2010.00706.x>
- Bloemendaal N, Muis S, Haarsma RJ, et al (2019) Global modeling of tropical cyclone storm surges using high-resolution forecasts. *Clim Dyn* 52:5031–5044. <https://doi.org/10.1007/s00382-018-4430-x>
- 740 Bossak BH, Keihany SS, Welford MR, Gibney EJ (2014) Coastal georgia is not immune: Hurricane history, 1851–2012. *Southeast Geogr* 54:323–333. <https://doi.org/10.1353/sgo.2014.0027>

Codiga DL (2021) UTide Unified Tidal Analysis and Prediction Functions

Codiga DL (2011) Unified Tidal Analysis and Prediction Using the UTide Matlab Functions. 59.
<https://doi.org/10.13140/RG.2.1.3761.2008>

745 Davis JL, Vinogradova NT (2017) Causes of accelerating sea level on the East Coast of North America. *Geophys Res Lett* 44:5133–5141. <https://doi.org/10.1002/2017GL072845>

Defne Z, Haas KA, Fritz HM (2009) Wave power potential along the Atlantic coast of the southeastern USA. *Renew Energy* 34:2197–2205. <https://doi.org/10.1016/j.renene.2009.02.019>

750 Déqué M (2007) Frequency of precipitation and temperature extremes over France in an anthropogenic scenario: Model results and statistical correction according to observed values. *Glob Planet Change* 57:16–26.
<https://doi.org/10.1016/j.gloplacha.2006.11.030>

Dietrich JC, Westerink JJ, Kennedy AB, et al (2011) Hurricane Gustav (2008) Waves and Storm Surge: Hindcast, Synoptic Analysis, and Validation in Southern Louisiana. *Mon Weather Rev* 139:2488–2522.
<https://doi.org/10.1175/2011MWR3611.1>

755 Dietrich JC, Zijlema M, Westerink JJ, et al (2011) Modeling hurricane waves and storm surge using integrally-coupled, scalable computations. *Coast Eng* 58:45–65. <https://doi.org/10.1016/J.COASTALENG.2010.08.001>

Domingues R, Goni G, Baringer M, Volkov D (2018) What Caused the Accelerated Sea Level Changes Along the U.S. East Coast During 2010–2015? *Geophys Res Lett* 45:13,367–13,376. <https://doi.org/10.1029/2018GL081183>

Doran KS, Long JW, Birchler JJ, et al (2022) Lidar-derived beach morphology (dune crest, dune toe, and shoreline) for U.S. sandy coastlines

760 Doran KS, Long JW, Overbeck JR (2015) A method for determining average beach slope and beach slope variability for U.S. sandy coastlines.

Dullaart JCM, Muis S, Bloemendaal N, Aerts JCJH (2020) Advancing global storm surge modelling using the new ERA5 climate reanalysis. *Clim Dyn* 54:1007–1021. <https://doi.org/10.1007/s00382-019-05044-0>

765 Egbert GD, Erofeeva SY, Ray RD (2010) Assimilation of altimetry data for nonlinear shallow-water tides: Quarter-diurnal tides of the Northwest European Shelf. *Cont Shelf Res* 30:668–679.
<https://doi.org/https://doi.org/10.1016/j.csr.2009.10.011>

Ezer T, Atkinson LP (2014) Accelerated flooding along the U.S. East Coast: On the impact of sea-level rise, tides, storms, the Gulf Stream, and the North Atlantic Oscillations. *Earth's Futur* 2:362–382. <https://doi.org/10.1002/2014ef000252>

770 Ezer T, Atkinson LP, Corlett WB, Blanco JL (2013) Gulf Stream's induced sea level rise and variability along the U.S. mid-Atlantic coast. *J Geophys Res Ocean* 118:685–697. <https://doi.org/10.1002/jgrc.20091>

Farris AS, Weber KM, Doran KS, List JH (2018) Comparing methods used by the U.S. Geological Survey Coastal and Marine Geology Program for deriving shoreline position from lidar data: U.S. Geological Survey Open-File Report 2018–1121

FEMA (2015) Guidance for Flood Risk Analysis and Mapping Coastal Wave Setup. 28

- 775 Fewtrell TJ, Bates PD, Horritt M, Hunter NM (2008) Evaluating the effect of scale in flood inundation modelling in urban environments. *Hydrol Process* 22:5107–5118. <https://doi.org/10.1002/hyp.7148>
- GEBCO (2014) The GEBCO 2014 Grid. https://www.gebco.net/news_and_media/gebco_2014_grid.html
- Georgas N, Yin L, Jiang Y, et al (2016) An open-access, multi-decadal, three-dimensional, hydrodynamic hindcast dataset for the Long Island sound and New York/New Jersey Harbor estuaries. *J Mar Sci Eng* 4:
780 <https://doi.org/10.3390/jmse4030048>
- Haiden T, Janousek M, Vitart F, et al (2019) Evaluation of ECMWF forecasts, including the 2019 upgrade | ECMWF
- Hayes MO (1979) Barrier Island Morphology as a Function of Tidal and Wave Regime. In: Leatherman SP (ed) *Barrier Islands*. Academic Press, pp 1–27
- Hersbach, H., Bell, B., Berrisford, P., Biavati, G., Horányi, A., Muñoz Sabater, J., Nicolas, J., Peubey, C., Radu, R., Rozum,
785 I., Schepers, D., Simmons, A., Soci, C., Dee, D., Thépaut J-N (2020) ERA5 hourly data on single levels from 1979 to present. In: Copernicus Clim. Chang. Serv. Clim. Data Store.
<https://cds.climate.copernicus.eu/cdsapp#!/dataset/reanalysis-era5-single-levels?tab=overview>. Accessed 11 Jan 2020
- Hersbach H, Bell B, Berrisford P, et al (2018) ERA5 hourly data on single levels from 1959 to present. In: Copernicus Clim. Chang. Serv. Clim. Data Store. <https://cds.climate.copernicus.eu/cdsapp#!/dataset/reanalysis-era5-single-levels?tab=form>
790
- Horsburgh KJ, Wilson C (2007) Tide-surge interaction and its role in the distribution of surge residuals in the North Sea. 112:1–13. <https://doi.org/10.1029/2006JC004033>
- Idier D, Bertin X, Thompson P, Pickering MD (2019) Interactions Between Mean Sea Level , Tide , Surge , Waves and Flooding : Mechanisms and Contributions to Sea Level Variations at the Coast. *Surv Geophys* 40:1603–1630.
795 <https://doi.org/10.1007/s10712-019-09549-5>
- Irish JL, Resio DT, Ratcliff JJ (2008) The influence of storm size on hurricane surge. *J Phys Oceanogr* 38:2003–2013. <https://doi.org/10.1175/2008JPO3727.1>
- Kenigson JS, Han W, Rajagopalan B, et al (2018) Decadal shift of NAO-linked interannual sea level variability along the U.S. northeast coast. *J Clim* 31:4981–4989. <https://doi.org/10.1175/JCLI-D-17-0403.1>
- 800 Kernkamp HWJ, Van Dam A, Stelling GS, De Goede ED (2011) Efficient scheme for the shallow water equations on unstructured grids with application to the Continental Shelf. *Ocean Dyn* 61:1175–1188.
<https://doi.org/10.1007/s10236-011-0423-6>
- Kernkamp HWJ, Van Dam A, Stelling GS, De Goede ED (2011) Efficient scheme for the shallow water equations on unstructured grids with application to the Continental Shelf. *Ocean Dyn* 61:1175–1188.
805 <https://doi.org/10.1007/s10236-011-0423-6>

- Kirezci E, Young IR, Ranasinghe R, et al (2020) Projections of global-scale extreme sea levels and resulting episodic coastal flooding over the 21st Century. *Sci Rep* 10:1–12. <https://doi.org/10.1038/s41598-020-67736-6>
- Kopp RE (2013) Does the mid-Atlantic United States sea level acceleration hot spot reflect ocean dynamic variability? *Geophys Res Lett* 40:3981–3985. <https://doi.org/10.1002/grl.50781>
- 810 Lin N, Emanuel K (2016) Grey swan tropical cyclones. *Nat Clim Chang* 6:106–111. <https://doi.org/10.1038/nclimate2777>
- Lin N, Emanuel KA, Oppenheimer M, Vanmarcke E (2012) Physically-based Assessment of Hurricane Surge Threat under Climate Change. *Nat Clim Chang* 2.6:462–467
- Lin N, Marsooli R, Colle BA (2019) Storm surge return levels induced by mid-to-late-twenty-first-century extratropical cyclones in the Northeastern United States. *Clim Change* 154:143–158. <https://doi.org/10.1007/s10584-019-02431-8>
- 815 Lyard FH, Allain DJ, Cancet M, et al (2021) FES2014 global ocean tide atlas: Design and performance. *Ocean Sci* 17:615–649. <https://doi.org/10.5194/os-17-615-2021>
- Lyard F, Lefevre F, Letellier T, Francis O (2006) Modelling the global ocean tides: Modern insights from FES2004. *Ocean Dyn* 56:394–415. <https://doi.org/10.1007/s10236-006-0086-x>
- 820 Maraun D, Wetterhall F, Ireson AM, et al (2010) Precipitation downscaling under climate change: Recent developments to bridge the gap between dynamical models and the end user. *Rev Geophys* 48:1–34. <https://doi.org/10.1029/2009RG000314>
- Marsooli R, Lin N (2018) Numerical modeling of historical storm tides and waves and their interactions along the U.S. East and Gulf Coasts. *J Geophys Res Ocean* 123:3844–3874. <https://doi.org/10.1029/2017JC013434>
- 825 Melet A, Meyssignac B, Almar R, Cozannet G Le (2018) Under-estimated wave contribution to coastal sea-level rise Underestimated wave contribution to coastal sea level rise. *Nat Clim Chang* 8:. <https://doi.org/10.1038/s41558-018-0088-y>
- Muis S, Apecechea MI, Álvarez, et al (2022) Global sea level change time series from 1950 to 2050 derived from reanalysis and high resolution CMIP6 climate projections. In: Copernicus Clim. Chang. Serv. Clim. Data Store. <https://cds.climate.copernicus.eu/cdsapp#!/dataset/sis-water-level-change-timeseries-cmip6?tab=overview>
- 830 Muis S, Apecechea MI, Dullaart J, et al (2020) A High-Resolution Global Dataset of Extreme Sea Levels, Tides, and Storm Surges, Including Future Projections. *Front Mar Sci* 7:1–15. <https://doi.org/10.3389/fmars.2020.00263>
- Muis S, Lin N, Verlaan M, et al (2019) Spatiotemporal patterns of extreme sea levels along the western North-Atlantic coasts. *Sci Rep* 9:1–12. <https://doi.org/10.1038/s41598-019-40157-w>
- 835 Muis S, Verlaan M, Nicholls RJ, et al (2017) A comparison of two global datasets of extreme sea levels and resulting flood exposure. *Earth's Futur* 5:379–392. <https://doi.org/10.1002/2016EF000430>
- Muis S, Verlaan M, Winsemius HC, et al (2016) A global reanalysis of storm surges and extreme sea levels. *Nat Commun* 7:1–11. <https://doi.org/10.1038/ncomms11969>

- NOAA (2009) Sea level variations of the united states 1854-2006. Silver Spring, Maryland
- 840 Olabarrieta M, Warner JC, Kumar N (2011) Wave-current interaction in Willapa Bay. *J Geophys Res* 116:C12014.
<https://doi.org/10.1029/2011JC007387>
- Parker K, Hill DF (2017) Evaluation of bias correction methods for wave modeling output. *Ocean Model* 110:52–65.
<https://doi.org/10.1016/j.ocemod.2016.12.008>
- Pawlowicz R, Beardsley B, Lentz S (2002) Classical tidal harmonic analysis including error estimates in MATLAB using T_TIDE. *Comput Geosci* 28:929–937. [https://doi.org/10.1016/S0098-3004\(02\)00013-4](https://doi.org/10.1016/S0098-3004(02)00013-4)
- 845 Rivas MB, Stoffelen A (2019) Characterizing ERA-Interim and ERA5 surface wind biases using ASCAT. 831–852
- Ruggiero P (2013) Is the Intensifying Wave Climate of the U.S. Pacific Northwest Increasing Flooding and Erosion Risk Faster Than Sea-Level Rise? *J Waterw Port, Coastal, Ocean Eng* 139:88–97.
[https://doi.org/10.1061/\(ASCE\)WW.1943-5460.0000172](https://doi.org/10.1061/(ASCE)WW.1943-5460.0000172)
- 850 Seifi F, Deng X, Andersen OB (2019) Assessment of the accuracy of recent empirical and assimilated tidal models for the Great Barrier Reef, Australia, using satellite and coastal data. *Remote Sens* 11:. <https://doi.org/10.3390/rs11101211>
- Serafin KA, Ruggiero P (2014) Simulating extreme total water levels using a time-dependent, extreme value approach. *J Geophys Res Ocean* 119:6305–6329. <https://doi.org/10.1002/2014JC010093>
- 855 Serafin KA, Ruggiero P, Stockdon HF (2017) The relative contribution of waves, tides, and non-tidal residuals to extreme total water levels on US West Coast sandy beaches. *Geophys Res Lett* 44:1839–1847.
<https://doi.org/10.1002/2016GL071020>
- Stammer D, Ray RD, Andersen OB, et al (2014) Accuracy assessment of global barotropic ocean tide models. *Rev Geophys* 52:243–282. <https://doi.org/10.1002/2014RG000450>
- Stockdon HF, Sallenger AH, Holman RA, Howd PA (2007) A simple model for the spatially-variable coastal response to hurricanes. *Mar Geol* 238:1–20. <https://doi.org/10.1016/j.margeo.2006.11.004>
- 860 Sweet WV, Hamlington BD, Kopp RE, et al (2022) Global and Regional Sea Level Rise Scenarios for the United States: Updated Mean Projections and Extreme Water Level Probabilities Along U.S. Coastlines. Silver Spring, MD
- Sweet W V., Park J, Gill S, Marra J (2015) New ways to measure waves and their effects at NOAA tide gauges: A Hawaiian-network perspective. *Geophys Res Lett* 42:9355–9361. <https://doi.org/10.1002/2015GL066030>
- 865 Timmermans BW, Gommenginger CP, Dodet G, Bidlot JR (2020) Global Wave Height Trends and Variability from New Multimission Satellite Altimeter Products, Reanalyses, and Wave Buoys. *Geophys Res Lett* 47:.
<https://doi.org/10.1029/2019GL086880>
- Titus JG, Hudgens DE, Trescott DL, et al (2009) State and local governments plan for development of most land vulnerable to rising sea level along the US Atlantic coast *. *Environ Res Lett* 4:. <https://doi.org/10.1088/1748-9326/4/4/044008>

- 870 US Census (2021) County Population Totals: 2010-2019. <https://www.census.gov/data/tables/time-series/demo/popest/2010s-counties-total.html>
- Veeramony J, Condon A, Van Ormondt M (2017) Forecasting Storm Surge and Inundation : Model Validation. *Weather Forecast* 32:2045–2063. <https://doi.org/10.1175/WAF-D-17-0015.1>
- Vousdoukas MI, Voukouvalas E, Mentaschi L, et al (2016) Developments in large-scale coastal flood hazard mapping. *Nat Hazards Earth Syst Sci* 16:1841–1853. <https://doi.org/10.5194/nhess-16-1841-2016>
- 875 Wahl T (2017) Sea-level rise and storm surges, relationship status: Complicated! *Environ Res Lett* 12:111001. <https://doi.org/10.1088/1748-9326/aa8eba>
- Wahl T, Haigh ID, Nicholls RJ, et al (2017) Understanding extreme sea levels for broad-scale coastal impact and adaptation analysis. *Nat Commun* 8:1–12. <https://doi.org/10.1038/ncomms16075>
- Wahl T, Mudersbach C, Jensen J (2011) Assessing the hydrodynamic boundary conditions for risk analyses in coastal areas: A stochastic storm surge model. *Nat Hazards Earth Syst Sci* 11:2925–2939. <https://doi.org/10.5194/nhess-11-2925-2011>
- 880 Wahl T, Plant N, Long JW (2016) *Journal of Geophysical Research : Oceans in the northern Gulf of Mexico*. 3029–3043. <https://doi.org/10.1002/2015JC011482>.Received
- Wang C, Song Z, Qiao F, Dong S (2009) What Signals Are Removed and Retained by Using an Anomaly Field in Climatic Research? *Int J Oceanogr* 2009:1–7. <https://doi.org/10.1155/2009/329754>
- 885 Ward PJ, Jongman B, Salamon P, et al (2015) Usefulness and limitations of global flood risk models. *Nat Clim Chang* 5:712–715. <https://doi.org/10.1038/nclimate2742>
- Wdowinski S, Bray R, Kirtman BP, Wu Z (2018) Increasing flooding hazard in coastal communities due to rising sea level : Case study of Miami Beach , Florida Ocean & Coastal Management Increasing fl ooding hazard in coastal communities due to rising sea level : Case study of Miami Beach , Florida. <https://doi.org/10.1016/j.ocecoaman.2016.03.002>
- 890 Weisberg RH, Zheng L (2008) Hurricane storm surge simulations comparing three-dimensional with two-dimensional formulations based on an Ivan-like storm over the Tampa Bay, Florida region. *J Geophys Res Ocean* 113:1–17. <https://doi.org/10.1029/2008JC005115>
- 895 Weisse R, Bellafiore D, Menéndez M, et al (2014) Changing extreme sea levels along European coasts. *Coast Eng* 87:4–14. <https://doi.org/10.1016/j.coastaleng.2013.10.017>
- Woodworth PL, Melet A, Marcos M, et al (2019) *Forcing Factors Affecting Sea Level Changes at the Coast*. Springer Netherlands
- 900 Ye F, Zhang YJ, Yu H, et al (2020) Simulating storm surge and compound flooding events with a creek-to-ocean model: Importance of baroclinic effects. *Ocean Model* 145:101526. <https://doi.org/10.1016/j.ocemod.2019.101526>

Yin J, Goddard PB (2013) Oceanic control of sea level rise patterns along the East Coast of the United States. *Geophys Res Lett* 40:5514–5520. <https://doi.org/10.1002/2013GL057992>

Zhao J, Johns W (2014) Wind-forced interannual variability of the Atlantic Meridional Overturning Circulation at 26.5 N. *J Geophys Res Ocean* 3909–3925. <https://doi.org/10.1002/2013JC009563>